NOTICE: The current controlled version of this document is on the LCODocs website (http://lcodocs.lanl.gov/). A printed copy of the document may not be the current version.

LOS ALAMOS NATIONAL LABORATORY
CARLSBAD OPERATIONS

LA-UR-25-30095

LCO-ACP-42, Revision 0

Neptunium (V) Solubility in WIPP Brine: Presence and Absence of WIPP-Relevant Organic and Inorganic Ligands

Effective Date: 03/31/2025

Originator:

Ugras Kaplan
Digitally signed by Ugras Kaplan
Date: 2025.03.28 16:03:36 -06'00'

Ugras Kaplan, LANL-CO ACRSP Date

Approved by:

Jonathan Icenhower
Digitally signed by Jonathan Icenhower
Date: 2025.03.31 09:05:31 -06'00'

Jonathan Icenhower, LANL-CO ACRSP Team Leader Date

PRISCILLA YANEZ (Affiliate)
Digitally signed by PRISCILLA YANEZ (Affiliate)
Date: 2025.03.31 09:27:07 -06'00'

Priscilla Yanez, LANL-CO Quality Assurance Manager Date

DOUGLAS WEAVER (Affiliate)
Digitally signed by DOUGLAS WEAVER (Affiliate)
Date: 2025.03.31 10:29:12 -06'00'

Douglas Weaver, LANL-CO Division Leader Date

History of Revisions

Revision Number	Effective Date	Pages Affected	Description of Revision
0	03/31/2025	All	Original Release

Table of Contents

ACRONYMS AND ABBREVIATIONS 7
1.0 INTRODUCTION 10
2.0 EXPERIMENTAL 13
2.1 Chemicals 13
2.2 Brine Solutions 14
2.3 ^{237}Np Stock Solution 14
2.4 Sample Matrix 15
2.5 pH and E_h measurement 17
2.6 Liquid phase characterization 18
2.7 Characterization of solid phase: XAS (X-Ray Absorption Spectroscopy) 18
3.0 RESULTS & DISCUSSION 19
3.1 Liquid phase speciation by UV-Vis-NIR 19
3.2 Solubility results 21
3.3 Solid phase speciation by XAS 28
4.0 CONLUSION 34
5.0 QUALITY ASSURANCE, DATA TRACEABILITY AND DOCUMENTATION 35
6.0 APPENDIX 35
6.1 Np(V) UV-Vis-NIR Spectra 35
7.0 REFERENCES 36

List of Tables

Table 1. Target and weighed concentrations of WIPP brine components used in Np solubility experiments [ACP-EXP-001] 14

Table 2. Experimental matrix for Solubility of Np(V) under WIPP-relevant Conditions studies 15

Table 3. Experimental matrix for screening experiments with organic complexants studies 16

Table 4. Experimental matrix for relative impacts of borate studies 16

Table 5. Experimental matrix for relative impacts of carbonate studies 17

Table 6. Distributions of dissolved Np(V) species in GWB, specifying $KNpO_2CO_3$ as the solubility-controlling solid, as modeled with EQ3/6 geochemical equilibrium modeling code [Domski and Sisk-Scott 2019] 23

Table 7. Energy positions of the Np L_{III}-edge XANES first inflection point and white line maximum for aqueous and solid Np(V) references and the seven samples investigated in the present work and two reference spectrum (Np(IV) and Np(V)). All values are given in eV (estimated calibration error ΔE ± 0.4 eV). p.w. = present work 30

Table 8. Best-fit of Np L_{III}–edge EXAFS model parameters ($S02$(k) = 0.9 fixed) 33

List of Figures

Figure 1. NIR absorption spectra of supernatant in contact with $NpO_2OH_{(am, fresh)}$ in 5.0 M NaCl , synthetic WIPP brine and synthetic WIPP brine without borate at pC_{H+} 7 (a) and 9 (b). 19

Figure 2. NIR absorption spectra of supernatant solutions in equilibrium with $NpO_2OH_{(am, fresh)}$ as a function of borate concentration in 5.0 M NaCl a) at pC_{H+} 7 and b) at pC_{H+} 9. 20

Figure 3. Solubility of $NpO_2(OH)_{(am, fresh)}$ in the absence and presence of organic ligands (citrate: 2.30 ×10^{-3} M, acetate: 2.83 ×10^{-2} M, oxalate: 1.13 × 10^{-2} M, EDTA: 7.92 × 10^{-5} M), and carbonate (16 ×10^{-3} M) in synthetic WIPP brine and 5M NaCl solutions as a function of time (a) and pC_{H+} (b). The maximum uncertainty is ± 15 %. 22

Figure 4. Solubility of NpO_2(OH)(aged) in the absence and presence of organic ligands (citrate: 2.30 × 10^{-3} M, acetate: 2.83 × 10^{-2} M, EDTA: 7.92 × 10^{-5} M) in 5 M NaCl solutions at $pC_{H+} \approx 9$ after 950 days. Red bars represent experimental values; blue bars show calculated solubility of NpO_2(OH)(aged) using the THEREDA TBD (Thermodynamic database), green bars show calculated solubility using the TC11a (ThermoChimie version 11a) TDB. 24

Figure 5. Solubility of $NpO_2(OH)_{(am)}$ in the presence of $[B]_{tot}$ ($0 \leq [B]_{tot} \leq 160$ mM) in 5 M NaCl solutions as a function of pC_{H+} determined in herein (as colored triangles), as well as previous experimental solubility data in the presence and absence of borate [Petrov et al. 2017; Hinz et al. 2020) (half-shaded diamonds) (a). The solubility of $NpO_2(OH)_{(am)}$ in synthetic WIPP brine in the presence and absence of 160 mM M borate as a function of pC_{H+} is also illustrated (b). The maximum uncertainty is ± 15 %. 26

Figure 6. Solubility of $NpO_2(OH)_{(am)}$ in the presence of 1 mM M ≤ $[CO_3^{-2}]_{tot}$ ≤ 100 mM in 5 M NaCl function of pC_{H+}. The results obtained with a maximum error rate of ± 15 %. 28

Figure 7. Np L_{III}–edge XANES spectra of Np(IV)O_2(cr) and Np(V)O_2(OH)(am) solid references used in the LCF analysis, as well as aqua reference XANES spectra of Np(IV)$O2$ +(aq) and Np(V)$O22$ +(aq) are shown for comparison purpose [Reich et al. 2000]. p.w. = present work. 29

Figure 8. Experimental Np-L_{III}-edge XANES spectra. Each experimental data are compared to corresponding linear combination fits of Np(IV)$O_{2(s)}$ reference and Np(V)$O_2(OH)_{(s)}$ reference. Linear combination fit = red, black = data. The limits of the LCF analysis applied to vertical, purple-colored stripes are shown. 29

Figure 9. Panel a: Np L_{III}-edge EXAFS spectra with corresponding EXAFS Fourier transform (FT): exp. (experimental) data and best fit of investigated sample Np(V) in synthetic WIPP brine at pC_{H+} 9 with 16 mM carbonate with considering Np-C shell. Panel b: same sample but not considering Np-C shell

during EXAFS calculation. Panel C: Np L_{III}-edge EXAFS spectra with corresponding EXAFS Fourier transform (FT): exp. data and best fit of investigated sample Np(IV)O_2(cr). Data magnitude (mag) (black), model magnitude (blue), data real part (red) and model real part (green). Also shown are single scattering paths......32

Figure 10: UV-Vis-NIR spectra of Np stock solution in 1 M HCl......35

EXECUTIVE SUMMARY

The oxidation state and solubility of neptunium (Np) in 5 M NaCl and high ionic strength synthetic WIPP (Waste Isolation Pilot Plant) brines were systematically investigated as a function of pC_{H+} (7-11) in the presence and absence of WIPP-relevant organic ligands, including EDTA (Ethylenediaminetetraacetic acid), oxalate, citrate, and acetate, as well as inorganic ligands such as borate and carbonate at a temperature of 23 ± 2°C. This study was conducted through long-term batch solubility experiments spanning approximately 950 days, using an undersaturation approach. A comprehensive set of experimental and spectroscopic techniques, including UV-VIS-NIR spectroscopy and Np L_{III}-edge X-ray Absorption Spectroscopy (XAS), was employed to identify the solubility-controlling Np solid phases and the predominant aqueous Np species present in the samples.

The results confirmed a significant impact of borate on the aqueous speciation and solubility of Np(V) in 5 M NaCl at pC_{H+} 9. The interactions of organic ligands with Np(V) were observed to differ between 5 M NaCl and synthetic WIPP brines. In the WIPP brine, the kinetics of the interactions varied, with these effects diminishing over time. In contrast, the interactions of organic ligands in 5 M NaCl were more stable. Additionally, the effect of carbonate on Np(V) solubility was most pronounced at pC_{H+} values of 9 and 11. Model calculations indicated that the total soluble Np species at pC_{H+} 9.3 should be 4.02×10^{-7} M under repository-relevant conditions, which is consistent with the concentration determined in these experiments: $3.84 \times 10^{-7} \pm 1.35 \times 10^{-8}$ M [Domski and Sisk-Scott 2019].

Another key finding of this study was that both the liquid phase, analyzed by UV-Vis, and the solid phase, measured by X-Ray Absorption Near Edge Spectroscopy (XANES), confirmed that Np maintained its dominant +V oxidation state across the phases under investigation. Solid-phase characterization through Extended X-ray Absorption Fine Structure (EXAFS) analysis revealed that the redox-controlling solid phase consisted of $KNpO_2CO_3(s)$ or $K_3NpO_2(CO_3)_2$, which also aligns with the predictions of the WIPP model [Domski and Sisk-Scott 2019].

The data generated from this study quantify the effects of organic compounds, borate, and carbonate on the solubility of Np(V), thereby providing empirical validation for the WIPP actinide model. The results will play an important role in informing decisions and recommendations made in the upcoming recertification of the WIPP (CRA-2026). The experiments were conducted by the Los Alamos National Laboratory - Carlsbad Operations (LANL-CO) Actinide Chemistry and Repository Science Program (ACRSP) as part of a broader initiative to establish realistic parameters related to actinide chemistry within the current WIPP Performance Assessment (PA) model and to enhance the conceptual model for WIPP chemistry in support of ongoing recertification efforts. These experiments were performed in compliance with the U.S. Department of Energy-Carlsbad Field Office (US DOE-CBFO) approved test plan, “Experimental Strategy to Challenge Actinide Solubility Predictions” (LCO-ACP-26). All data reported were generated under the LANL-CO WIPP Quality Assurance (QA) Program, adhering to the DOE-CBFO Quality Assurance Program Document (QAPD). In addition to this interim report, the 950-day solubility experiments will be continued, further characterization studies will be conducted, and more comprehensive results will be obtained to prepare the final report.

ACRONYMS AND ABBREVIATIONS

^{241}Am	Americium 241
Ac.	Acetate: CH_3COOH
ACRSP	Actinide Chemistry and Repository Science Program
am	amorphous solid
An	Actinide
An(IV)	Tetravalent actinide
An(V)	Pentavalent actinide
ANL	Argonne National Laboratory
APS	Advance Photon Source
aq	Aqueous
°C	Celsius
CO_2	Carbon dioxide
Ca	Calcium
$CaCl_2$	Calcium chloride
CBFO	Carlsbad Field Office (U.S. Department of Energy)
Cl^-	Chlorine
Cit.	Citrate: $C_6H_8O_7$
CO_3^{2-}	Carbonate
CPR	Cellulosic, Plastic, and Rubber materials
cr	Crystalline
CRA	Compliance Recertification Application
DOE	Department of Energy
EDTA	Ethylenediaminetetraacetic acid: $C_{10}H_{16}N_2O_8$
EQ3/6	Software program for geochemical modeling of aqueous systems
ERDA-6	U.S. Energy Research and Development Administration Well 6, a synthetic brine representative of fluids in Castile brine reservoirs
eV	Electron volt
EXAFS	Extended X-ray Absorption Fine Structure
Exp	Experimental
FT	Fourier transform
Ge	Germanium
GWB	Generic Weep Brine, a synthetic brine representative of intergranular Salado-Formation brines
H^+	Hydronium
HBr	Hydrogen Bromide
H_2O	Water
HCO_3^-	Bicarbonate

ACRONYMS AND ABBREVIATIONS (cont.)

HNO_3	Nitric acid
HPW	high purity water
ICP-MS	Inductively Coupled Plasma-Mass Spectrometer
I_{tot}	Total ionic strength
kDa	Kilodalton
kg	Kilogram
LANL-CO	Los Alamos National Laboratory−Carlsbad Operations
LCFA	Linear Combination Fit Analysis
M	Molarity, moles of solute per liter of solvent
$MgCl_2$	Magnesium chloride
mg	Milligram
mL	Milliliter
Mg	Magnesium
$MgCO_3^-$	Magnesium carbonate
MgO	Magnesium oxide
mM	Millimolar
Na^+	Sodium ion
$NaC1O_4$	Sodium perchlorate
NaCl	Sodium chloride
$NaHCO_3$	Sodium hydrogen carbonate
Nd(III)	Trivalent Neodymium
NIR	Near Infrared
nm	Nano meter
Np(III)	Trivalent Neptunium ion
Np(IV)	Tetravalent Neptunium ion
Np(V)	Pentavalent Neptunium ion
Np(VI)	Hexavalent Neptunium ion
OH^-	Hydroxide ion
Ox.	Oxalic acid: $H_2C_2O_4$
PA	Performance Assessment
pC_{H+}	Negative logarithm of H^+ concentration in moles/liter
pH	Negative logarithm of H^+ activity
pH_{exp}	The experimentally measured pH
pH_m	The measured pH
ppb	Parts per billion
ppm	Parts per million (Microgram/gram)

ACRONYMS AND ABBREVIATIONS (cont.)

p.w.	Present work
QA	Quality Assurance
QAPD	Quality Assurance Program Document
rpm	Revolutions per minute
SOTERM	Actinide Source Term (appendix in the WIPP CRA)
SEM-EDS	Scanning electron microscopy (SEM) and energy dispersive spectroscopy
Si	Silicon
T	Temperature
TRU	Transuranic Element (actinides higher in atomic number than uranium)
US	United States
UV–Vis-NIR	Ultraviolet/Visible/Near Infrared Spectroscopy
WIPP	Waste Isolation Pilot Plant
XAS	X-ray absorption spectroscopy
XANES	X-ray absorption near edge spectroscopy
XPS	X-ray photoelectron spectroscopy
XRD	X-Ray Diffraction
λ_{max}	Maximum wavelength of absorption
Zr	Zirconium

1.0 INTRODUCTION

The Waste Isolation Pilot Plant (WIPP) is the United States' sole deep geologic repository for high-level radioactive waste and the first such facility globally designed to dispose of defense-related transuranic (TRU) radioactive waste in a salt-based geologic medium. Located 2,150 feet underground in an ancient salt formation, WIPP permanently isolates defense-generated TRU waste [Kirkes and Patterson 2014, CRA 2014, Schramke et al. 2020]. Ensuring the safe disposal of this radioactive waste is imperative to prevent human and environmental exposure.

The potential for containment breaches, leading to the release of radionuclides and their subsequent migration through the surrounding geological matrix, is a critical consideration in safety assessments for waste repositories. The migration of actinides is governed by various geochemical processes, including redox transformations, colloid formation, sorption and precipitation, desorption and dissolution, solubility, and complexation with ligands. These processes are heavily influenced by the composition of intruding brine. A comprehensive understanding of the geochemistry of the repository waste forms is essential for accurately assessing the long-term performance of a radioactive waste disposal facility [Silva and Nitche 1995, Runde 2002, Runde 2000, Choppin 2007].

Within the actinide series, the pentavalent neptunium ion [Np(V)] is the most stable oxidation state in aqueous solutions. This stability makes Np(V) a key representative for studying the aqueous chemistry of all actinides in the (+V) oxidation state. In the context of the WIPP scenario, Np is particularly noteworthy, as it is the primary daughter product of americium-241 (^{241}Am) decay (via alpha decay and neutron capture), leading to an increase in its inventory over time. As such, Np becomes progressively more significant during the 10,000-year performance period of the repository.

Neptunium-237 (^{237}Np), with a half-life of 2.14×10^6 years, is one of the principal contributors to the radiotoxicity of spent nuclear fuel in a deep geologic repository after several centuries of storage. Neptunium is a redox-sensitive element, exhibiting complex chemical behavior and solubility characteristics. It can exist in five oxidation states, ranging from III to VII, in aqueous environments [Lemire 2001]. The electronic states and chemical speciation of Np are highly dependent on local geochemical conditions, including pH, redox potential (E_h), and ionic strength. Under reducing conditions typical of natural groundwater, Np(IV) predominates, whereas in more oxidizing waters, Np(V) is the most prevalent species. Np(IV) is significantly less soluble, forming hydroxo complexes that are approximately five orders of magnitude less soluble than the corresponding Np(V) complexes [Neck and Kim 2001, Silva and Nitche 1995, Kaszuba and Runde 1999].

Neptunium solubility in brines:

Solubility experiments are highly relevant to the PA of the near field of a nuclear waste repository in the event of a brine intrusion. In saline solutions, the aqueous Np(V) species are in equilibrium with redox-controlling solid phases, which are influenced by factors such as salt concentration, pH, the presence or absence of ligands, CO_2 partial pressure, and other parameters. The solubility and interaction behavior of the NpO_2^+ ion in single-component systems, such as $NaClO_4$ and NaCl solutions, in the presence and absence of carbonate has been described successfully by considering the interaction between NpO_2^+, OH^-, Cl^-, ClO_4^- and CO_3^{2-} [Neck et al. 1994, Fanghänel et al. 1995, Neck et al. 1995].

Novak et al. (1996) investigated the solubility behavior of Np(V) in three synthetic Na-K-Mg-Cl brines simulating WIPP conditions, with ionic strengths [I_{tot}] of 0.84, 2.97, and 7.78, respectively, in the presence of CO_2(g) using an oversaturation experimental approach. The pH value ranges from 7.1 to 7.5. Dissolved Np(V) concentrations decreased by several orders of magnitude within the first 100 days of the experiment. The solid phases formed in all experiments were identified as $KNpO_2CO_3 \bullet xH_2O_{(S)}$ by X-ray powder diffraction analysis [Novak et al. 1996a].

Organic effects:

Inorganic and organic ligands, through interactions with metals in aqueous solutions, can alter the oxidation state on one hand, and on the other hand, they can either increase or decrease the solubility of metals by forming complexes. They can also stabilize the new oxidation state which may precipitate to form a secondary solid phase [Runde 2000]. There are various organic components of nuclear wastes which are disposed in the WIPP repository. The complexation of NpO_2^+ with acetate, citrate, EDTA and oxalate have been studied in saline solutions [Novak et al. 1996b, Pokrovsky et al. 1998, Moore et al. 1999].

Reed et al. (1998) investigated the effects of oxalate, citrate, and EDTA on the oxidation state of Np(VI) in ERDA-6 at pC_{H+} 8 and10 in G-Seep (Salado) brine at pC_{H+} 5 and 7. The presence of organic complexants facilitated the rapid reduction of Np(VI) in G-Seep brine at pH values of 5 and 7. In contrast, at pH values of 8 and 10 in ERDA-6 brine, carbonate and hydrolytic complexes predominated, thereby inhibiting or slowing the reduction of Np(VI) by the organic ligands present. The author also discussed the competition between Np-organic and Np-carbonate complexation in the presence of carbonates in the system. Although Np(VI)-carbonate complexes were stable in the absence of organic ligands, the author reported that in the presence of both carbonates and organic ligands, Np(VI) was reduced to Np(V) and Np(IV). The reduction of Np(VI) was attributed to the presence of organic complexants in solution; in the absence of carbonates, the reduction to Np(V) and Np(IV), along with precipitation, occurred more rapidly [Reed et al. 1998].

Borate effects:

Brush (1989) reported borate present mainly as H_3BO_3 and $HB4\ O_7^-$ or H_3BO_3 and $B(OH)_4^-$ a naturally occurring compound in the Salado Formation brine. The concentration of borate in the intergranular brines at WIPP is approximately 160 mM, calculated as mono-boric acid, ranking just behind chloride and sulfate [Snider 2003, Brush 1989].

The speciation of borate in aqueous systems is highly complex, potentially influenced by factors such as pH, ionic strength, and total boron concentration. To date, only a limited number of experimental studies have been conducted on borate complexation with select lanthanides and actinides. Most of these studies focus on Nd(III), Eu(III), and Cm(III) as analogs for the trivalent actinides Am(III) and Pu(III). However, a systematic study of actinide-borate complexation remains to be performed [Schott et al. 2014, 2015; Hinz et al. 2015].

Hinz et al. (2020) investigated the interaction of borate ($[B]_{tot}$ = 0.004 M to 0.16 M) through a series of comprehensive solubility experiments conducted in 0.1–5.0 M NaCl and 0.25–4.5 M $MgCl_2$ solutions, with pH values ranging from 7.2 to 10.0 ($pH_m = -\log[H^+]$). The study employed various analytical techniques, including X-ray Photoelectron Spectroscopy (XPS), X-ray Diffraction (XRD), Scanning Electron Microscopy (SEM), Energy Dispersive X-ray Spectroscopy (EDS), Ultraviolet-Visible-Near Infrared (UV-Vis-NIR), and synchrotron-based spectroscopic techniques such as XAS. UV-Vis-NIR analysis clearly indicated the formation of weak Np(V)–borate complexes under mildly alkaline conditions, with polyborate species likely contributing to the complex formation. The presence of Np(V)–borate complexes was found to have a minimal effect on the solubility of Np(V) in near-neutral to weakly alkaline pH conditions. However, a significant reduction in Np(V) solubility (3 to 4 orders of magnitude) was observed in NaCl and dilute $MgCl_2$ solutions with $[B]_{tot}$ = 0.16 M and $pH_m \leq 9$. XRD, XPS, SEM–EDS, and XAS analyses confirmed the formation of previously unrecognized Na–Np(V)–borate(cr) and Mg–Np(V)–borate(cr) solid phases in NaCl and dilute $MgCl_2$ solutions, respectively. While undersaturation solubility experiments with the Mg–Np(V)–borate(cr) phase demonstrated very low solubility in 4.5 M $MgCl_2$ solutions, the transformation of NpO_2OH(am) was kinetically hindered and was not observed within the timeframe of this study in such concentrated brines [Hinz et al. 2020].

Carbonate effects:

Carbon dioxide (CO_2) will be produced at the WIPP by the assumed microbial degradation of coexisting cellulosic, plastic, and rubber (CPR) materials. The generated CO_2 has the potential to dissolve in brine and subsequently react with the engineered barrier material, magnesium oxide (MgO), leading to the formation of an insoluble magnesium carbonate ($MgCO_3$) compound. In addition, calcium and iron (II) are present within the WIPP and are capable of forming insoluble carbonates [Borkowski et al. 2009]. Previous studies have demonstrated that in carbonate-free solutions, solid phases such as NpO_2OH(s) and Np_2O_5(s) are thermodynamically stable [Lierse et al. 1985, Kaszuba and Runde 1999, Kim 2006). In contrast, in equilibrium conditions where

carbonate is present, the solubility-limiting solid phases are represented by $M_3NpO_2CO_3 \cdot xH_2O$ and $M_3NpO_2(CO_3)_2$ ($M = Na^+, K^+$), as evidenced by XRD analysis. Therefore, a critical characteristic of the solubility-limiting solid phases of Np(V) is their pronounced dependence on the concentration of alkali carbonates [Neck et al. 1994, Novak et al. 1997, Al Mahamid et al. 1998].

Experimental objectives and scope:

WIPP PA calculations require more detailed data on the solubilities of Np(V) in WIPP brines. A review of the literature reveals that a series of studies on the solubility and speciation of Np have generally been conducted in simple background electrolyte media such as $NaClO_4$, NaCl, $MgCl_2$, or $CaCl_2$, with the results primarily derived from these solutions [Shilov et al. 2012, Gaona et al. 2013, Hinz et al. 2015, Fellhauer et al. 2016, Petrov et al. 2017].

A well-established and systematic examination of these complicated environmental systems in the WIPP brines is crucial to describe the chemical behavior of the actinides sufficiently. Before the ternary system (actinide--brine component—ligand complexation) interaction can be described, the different binary systems, including actinide/brine, actinide/organic ligand and actinide/borate must be investigated.

The aqueous chemistry of Np(V) in 5 M NaCl and synthetic WIPP brines as a function of pC_{H^+} in presence and absence of borate, WIPP relevant ligands (EDTA, oxalate, citrate, acetate) and carbonate at $T = 23 \pm 2$ ∘C was thoroughly studied by long-term batch solubility experiments (approximately 950 days) from an undersaturation approach. The data obtained from this work quantify the effects of WIPP-relevant concentrations of organics, borate, and carbonate on the solubility of Np(V), which can then inform the WIPP actinide model and provide recommendations for future WIPP recertifications.

2.0 EXPERIMENTAL

2.1 Chemicals

NaCl, HNO_3, NaOH, HCl, $NaHCO_3$, $MgCl_2 \cdot 6H_2O$ $CaCl_2 \cdot 2H_2O$ $Na_2B_4O_7 \cdot 10H_2O$, LiCl, KCl, NaBr, Na_2SO_4 (Fisher Scientific), HBr, oxalate [disodium oxalate], EDTA [disodium EDTA$\cdot 2H_2O$] (Sigma-Aldrich), citrate [citric acid anhydrous] (Fluka), acetate [acetic acid], (Acros Organics) were used in this study. All solutions were prepared with high purity water (HPW, 18.2 MΩ-cm). All solutions and samples were prepared by first degassing HPW with nitrogen for 5-6 hours and then bringing it inside an inert gas (nitrogen) glovebox at 23 ± 2 °C. All brine preparations, final Np stock preparations, experimental setup, and sampling were conducted in a nitrogen atmosphere glovebox. Samples remained in the glovebox for the duration of the experiments. Oxygen partial pressure was kept below 10 ppm throughout the experiments. Samples were doubly contained in sealed vessels to prevent any exposure to oxygen and prevent sample evaporation. Also, dissolved oxygen in the solutions was measured with a Rhodazine test kit (CHEMetrics made in USA) (detection limit of 25 ppb) and found to be below detection limit.

2.2 Brine Solutions

The predicted range in brine composition expected in the WIPP is shown in Table 1. These brines are Na/Mg/Cl dominated with lesser amount of calcium, borate, sulfate, potassium, lithium, bromide, and carbonate. In long term experiments, 90% strength compositions are used to prevent salt precipitation and minimize mineral colloid and pseudo-colloid formation. This dilution is a necessary step for anoxic experiments. The 30 mL polypropylene bottles were conditioned with brine solutions for 2 weeks before experiments began.

Table 1. Target and weighed concentrations of WIPP brine components used in Np solubility experiments [ACP-EXP-001]

Ion	90% GWB* [I_{tot}]: 6.34 (M) ****		90% pC_{H+} 9 ** [I_{tot}]: 5.40 (M) ****		90% pC_{H+} 11*** [Itot]: 5.06 (M) ****		5 M NaCl [Itot]: 5.00 (M) ****	
	target	actual	target	actual	target	actual	target	actual
Li^+	3.89×10^{-3}	3.79×10^{-3}	3.38×10^{-3}	3.51×10^{-3}	3.19×10^{-3}	3.15×10^{-3}	-	-
Na^+	3.13	3.08	3.15	3.00	4.46	4.71	5.00	5.00
Mg^{2+}	9.01×10^{-1}	9.02×10^{-1}	9.27×10^{-1}	9.27×10^{-1}	9.99×10^{-3}	1.01×10^{-2}	-	-
K^+	4.14×10^{-1}	4.15×10^{-1}	4.12×10^{-1}	4.12×10^{-1}	4.04×10^{-1}	4.06×10^{-1}	-	-
Ca^{2+}	1.22×10^{-2}	1.22×10^{-2}	1.22×10^{-2}	1.21×10^{-2}	9.81×10^{-3}	9.87×10^{-3}	-	-
Cl^-	4.96	4.88	4.89	4.78	4.78	4.92	5.00	5.00
SO_4^{2-}	1.57×10^{-1}	1.58×10^{-1}	1.58×10^{-1}	1.51×10^{-1}	1.51×10^{-1}	1.57×10^{-1}	-	-
Br^-	2.36×10^{-2}	2.12×10^{-2}	2.12×10^{-2}	2.08×10^{-2}	2.07×10^{-2}	2.37×10^{-2}	-	-
$B_4O_7^{2-}$	3.49×10^{-2}	3.47×10^{-2}	3.50×10^{-2}	3.51×10^{-2}	2.75×10^{-2}	2.75×10^{-2}	-	-

*GWB: Generic Weep Brine.
** pC_{H+} 9: Specific brine at pH 9.
***pC_{H+} 11: Specific brine at pH 11.
****Ionic Strength calculated via the EQ3\6 software [Wolery 2008]. Using the Sandia National Laboratories FMT database [Xiong 2011].

2.3 ^{237}Np Stock Solution

The starting ^{237}Np material was obtained from Oak Ridge National Laboratory (ORNL) with a composition of ^{237}Np 99.99% (^{236}Np < 0.01% and ^{235}Np < 0.001%) in oxide form ($NpO_{2(s, cr)}$, batch ^{237}Np-4157). Approximately 75 mg $NpO_{2\ (s, cr)}$ was weighed and put in 5 mL concentrated HNO_3 (Fisher Scientific) to dissolve. The solution was then heated to dryness at 130 °C. The solid changed from black to dark green, indicating a shift in oxidation state from Np(IV) to Np(V) and Np(VI). Heating and drying were repeated 4 times with 5 mL 1 M HCl, after which 4 mL of 1 M $NaHCO_3$ (pH 9) was added. A white Na-NpO_2-CO_3 precipitate was observed and subsequently

separated by decanting [Neck 1995]. An aliquot (1–2) mL of the white $NaNpO_2CO_3$ suspension was dissolved with 5 mL 1 M HCl. The pH of the Np stock solution (< 1) was checked again to verify the solution did not contain any carbonate. At the end, a greenish color solution was observed. The oxidation state purity of this solution was confirmed by UV-vis spectroscopy. Spectrophotometric measurements were performed using a Cary 5000 (Varian) UV-Vis-NIR spectrometer in double-beam mode. Measurements were conducted in gas-tight cuvettes. Spectra were recorded with a 0.2 nm data interval, a scan rate of 60 nm•min^{-1} and a slit-width of 0.6 nm. The UV-Vis-NIR spectrum showed a main Np(V) peak at 981 nm [Petrov et al. 2017]. No peaks attributable to other Np oxidation states were observed. The UV-Vis-NIR spectrum of Np(V) in 1 molar HCl solution can be found in Figure 9 in the appendix section.

2.4 Sample Matrix

Aliquots of Np(V) stock solution were precipitated with carbonate-free 1 M NaOH. The resulting greenish $NpO_2OH_{(am)}$ solid was washed twice with high purity water that was adjusted to pH 10. The total mass of ^{237}Np in each sample was ~0.5 mg. For these experiments, samples were equilibrated in three synthetic WIPP brines, along with 5 M NaCl used as the background electrolyte. These include 5 M NaCl at pC_{H+} 7, 9, and 11, 90% GWB at pC_{H+} 7, and transitional brines at pC_{H+} 9 and 11. Samples were systematically monitored for pC_{H+}, E_h and aqueous Np concentration by Inductively Coupled Plasma-Mass Spectrometer (ICP-MS). The present work is divided into four subtasks. These subtasks and their sample matrix's will be presented in the next part.

Subtask 1: Solubility of Np(V) under WIPP-relevant Conditions

Table 2. Experimental matrix for Solubility of Np(V) under WIPP-relevant Conditions studies

ACRSP Experiment Designation	Ligands Present	pC_{H+} value at 950 days	Brine Type	Eh (mV) (800-950 days)
Np(V)-Brine	none	7.30	90% GWB	80
Np(V)-Brine	none	9.10	90% pC_{H+} 9	95
Np(V)-Brine	none	11.0	90% pC_{H+} 11	110
Np(V)-Organic	Acetate, Oxalate, Citrate, EDTA	6.85	90% GWB	-180
Np(V)-Organic	Acetate, Oxalate, Citrate, EDTA	9.15	90% pC_{H+} 9	-170
Np(V)-Organic	Acetate, Oxalate, Citrate, EDTA	11.05	90% pC_{H+} 11	-90
Np(V)-Carbonate	Carbonate	7.25	90% GWB	40
Np(V)-Carbonate	Carbonate	9.00	90% pC_{H+} 9	80
Np(V)-Carbonate	Carbonate	10.95	90% pC_{H+} 11	50
Np(V)- All	Acetate, Oxalate, Citrate, EDTA and Carbonate	7.00	90% GWB	-80

Table 2. Experimental matrix for Solubility of Np(V) under WIPP-relevant Conditions studies (cont.)

ACRSP Experiment Designation	Ligands Present	pC_{H+} value at 950 days	Brine Type	Eh (mV) (800-950 days)
Np(V)- All	Acetate, Oxalate, Citrate, EDTA and Carbonate	8.90	90% pC_{H+} 9	-100
Np(V)- All	Acetate, Oxalate, Citrate, EDTA and Carbonate	11.00	90% pC_{H+} 11	-50

* Acetate: 2.83×10^{-2} M, oxalate: 1.13×10^{-2} M, citrate: 2.30×10^{-3} M, ethylenediaminetetraacetic acid (EDTA): 7.92×10^{-5} M [Van Soest 2018].

Subtask 2: Screening Experiments with Organic Complexants

Table 3. Experimental matrix for screening experiments with organic complexants studies

ACRSP Experiment Designation	Ligands Present	pC_{H+} value at 950 days	Brine Type	Eh (mV) (800-950 days)
Np(V)-Control	none	7.30	5 M NaCl	-120
Np(V)-Ac	Acetate	9.10	5 M NaCl	-140
Np(V)-Ac	Acetate	11.0	90% pC_{H+} 9	-70
Np(V)-Ox	Oxalate	6.80	5 M NaCl	-100
Np(V)-Ox	Oxalate	9.10	90% pC_{H+} 9	-55
Np(V)-Cit	Citrate	11.0	5 M NaCl	-140
Np(V)-Cit	Citrate	7.20	90% pC_{H+} 9	-180
Np(V)-E	EDTA	9.0	5 M NaCl	-75
Np(V)-E	EDTA	10.9	90% pC_{H+} 9	10
Np(V)-ORG	Inventory-defined organics	7.00	5 M NaCl	-60

Subtask 3: Relative Impacts of Borate

Table 4. Experimental matrix for relative impacts of borate studies

ACRSP Experiment Designation	Ligands Present	pC_{H+} value at 950 days	Brine Type	Eh (mV) (800-950 days)
Np(V)-Control	no borate	7.20	5 M NaCl	-135
Np5-Control	no borate	11.30	5 M NaCl	-120
Np5-B-10	10 mM borate	7.10	5 M NaCl	-20
Np5-B-10	10 mM borate	9.30	5 M NaCl	-50
Np5-B-10	10 mM borate	11.20	5 M NaCl	45
Np5-B-50	50 mM borate	7.30	5 M NaCl	10
Np5-B-50	50 mM borate	9.00	5 M NaCl	40
Np5-B-50	50 mM borate	11.3	5 M NaCl	100
Np5-B-100	100 mM borate	7.00	5 M NaCl	120
Np5-B-100	100 mM borate	8.75	5 M NaCl	70

Table 4. Experimental matrix for relative impacts of borate studies (cont.)

ACRSP Experiment Designation	Ligands Present	pC_{H+} value at 950 days	Brine Type	Eh (mV) (800-950 days)
Np5-B-100	100 mM borate	11.20	5 M NaCl	150
Np5-B-160	160 mM borate	7.30	5 M NaCl	140
Np5-B-160	160 mM borate	9.20	5 M NaCl	170
Np5-B-160	160 mM borate	11.20	5 M NaCl	140
Np5-B-WIPP	borate free	7.20	90% pC_{H+} 7	30
Np5-B-WIPP	borate free	9.30	90% pC_{H+} 9	70
Np5-B-WIPP	borate free	11.00	90% pC_{H+} 11	50

Subtask 4: Relative Impacts of Carbonate

Table 5. Experimental matrix for relative impacts of carbonate studies

ACRSP Experiment Designation	Ligands Present	pC_{H+} value at 950 days	Brine Type	Eh (mV) (800-950 days)
Np5-C-1	1 mM carbonate	8.00	5 M NaCl	-100
Np5-C-1	1 mM carbonate	9.20	5 M NaCl	-40
Np5-C-1	1 mM carbonate	10.20	5 M NaCl	-80
Np5-C-5	5 mM carbonate	8.00	5 M NaCl	-100
Np5-C-5	5 mM carbonate	9.20	5 M NaCl	20
Np5-C-5	5 mM carbonate	10.50	5 M NaCl	-60
Np5-C-10	10 mM carbonate	8.00	5 M NaCl	-50
Np5-C-10	10 mM carbonate	9.30	5 M NaCl	-100
Np5-C-10	10 mM carbonate	10.40	5 M NaCl	40
Np5-C-100	100 mM carbonate	8.00	5 M NaCl	70
Np5-C-100	100 mM carbonate	9.50	5 M NaCl	10
Np5-C-100	100 mM carbonate	10.30	5 M NaCl	-30

2.5 pH and E_h measurement

Measurements of pH were made using a combination pH electrode (Orion ROSS). The hydrogen ion concentration (pC_{H+}= –log [H+], in molal units) was determined according to $pC_{H+} = pH_{exp} + \Delta pH$, as described previously in the literature [Altmaier et al. 2003, Borkowski et al. 2009], where pH_{exp} is the measured pH value and ΔpH is the empirical correction factor accounting for the liquid junction potential of the electrode and the activity coefficient of H^+. Values for ΔpH used in the present study were 0.86, 0.87, 1.12, and 1.11 for 5.0 M NaCl, pC_{H+} 11, pC_{H+} 9, and GWB (Generic Weep Brine), respectively.

Oxidation-reduction potential measurements were obtained using an Orion A221 meter equipped with a Mettler Toledo InLab glass redox microelectrode with a platinum ring. Corrections from

redox potential to E_h were made by adding the Ag/AgCl redox potential from the meter reading Zobell solution (LabChem). In E_h measurements, especially in solutions with high ionic strength, the uncertainty can be up to 200 mV. In order to perform more precise measurements and reduce the error, after each E_h measurement the electrode was washed with 1 M HCl, then water, then 1 M NaOH, and the final wash with water (total cleaning process time is 1-2 hours), and after every two or three measurements the electrode filling solution, 3 M KCl, was replaced with fresh solution [Altmaier et al. 2010].

2.6 Liquid phase characterization

Spectrophotometric measurements were performed using a Cary 5000 (Varian) UV-Vis-NIR spectrometer in double-beam mode. Measurements were conducted in gas-tight cuvettes. Spectra were recorded with a 0.2 nm data interval, a scan rate of 60 nm•min^{-1} and a slit-width of 0.6 nm. Sampling for NIR analysis was performed after 60 days. Selected samples with sufficient Np concentration were centrifuged in a glovebox through a 10 kDa filter (13,000 rpm) (Pall-type filters, Omega-modified polyethersulfone) prior to NIR measurements to separate suspended solid phase particles. Before using all the filters, they were cleaned by filtering three times with a 5 M NaCl solution to remove any impurities, and a pre-conditioning process was performed. Separate baselines were recorded for each pC_{H+}, ionic strength condition, and ligand concentration. Three absorption spectra were collected sequentially for each sample at 23 °C and merged into one spectrum as shown.

^{237}Np concentrations in brine solutions were analyzed by ICP-MS an Agilent 7900 after 10 kDa filtration. The neptunium standard used for calibration (1.013×10^{-6} Ci/g) was provided by Eckert & Zeigler radioisotopes, and the detection limit for Np is between 10^{-10} and 10^{-11} M.

2.7 Characterization of solid phase: XAS (X-Ray Absorption Spectroscopy)

X-ray Absorption Spectroscopy was performed at 10-BM beamline at the Advanced Photon Source (APS), Argonne National Laboratory (ANL) [Kropf et al. 2010]. Bulk XAS data at the Np L_{III}-edge at 17610 eV were collected in fluorescence mode at room temperature using a four-element Ge solid-state detector. The beamline is equipped with a Ge (422) double crystal water-chilled Si (311) double-crystal monochromator. Energy calibration was carried out after each sample by the measurement of a Zr foil (Zr K-edge at 17998 eV). The XANES data analysis was performed with the LARCH software program, where the average oxidation state of Np in the bulk XAS samples was determined by fitting the XANES region between 17,585 and 17,700 eV by a linear combination fit (LCF) of reference spectra for Np(IV) and Np(V) [Newville 2013].

Normalization, transformation from energy into K-space, subtraction of a spline background and shell fits, were performed with LARCH software program to execute the EXAFS analysis [Newville 2013] and FEFF8 [Ankudinov et al. 2002]. The single scattering phases and amplitudes were calculated using the crystal structure of NpO_2 to model Np-Np and Np-O_{eq} interaction for NpO_2(cr) sample [Zachariasen et al. 1949]. The crystal structure $KNpO_2CO_3$ was used to model

Np=O_{ax} Np-O_{eq}, Np-C, and Np-K interactions [Kuzenkova et al. 2023]. The theoretical models were fit to the K^2-weighted EXAFS spectra using an amplitude reduction factor of $S_0^2(k)= 0.9$.

3.0 RESULTS & DISCUSSION

3.1 Liquid phase speciation by UV-Vis-NIR

Aqueous Np species and oxidation states were investigated using UV-Vis-NIR after 60 days for samples in equilibrium with $Np(V)O_2OH_{(am)}$ in 5 M NaCl and synthetic WIPP brine with and without borate (pC_{H+} 7 and 9) . The NIR spectra of Np in the supernatant between 940 and 1040 nm are displayed in Figure 1. The absorption intensity of Np(V) at λ = 981–988 nm systematically decreases with increasing pC_{H+}, due to lower Np solubility under more alkaline conditions. We observed a peak shift of the Np(V) aquo ion in 5 M NaCl at pC_{H+} 7 and 9, indicative of contributions from Np(V) chloro-complexes, $NpO_2(OH_2)_{5-n}Cl_n^{1-n}$, and Np(V) hydrolysis species, and $NpO_2(OH_2)_{5-m}(OH)_{1-m}$, respectively. Similar results for Np(V) in NaCl and $CaCl_2$ solutions were reported in Fanghänel et al. 1995, Fellhauer et al. 2016, and Petrov et al. 2017.

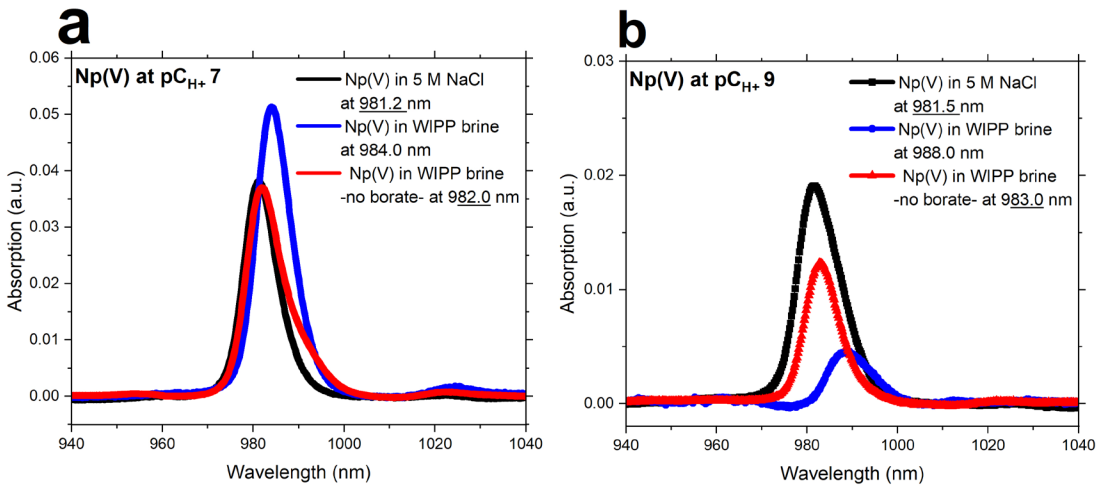


Figure 1. NIR absorption spectra of supernatant in contact with $NpO_2OH_{(am, fresh)}$ in 5.0 M NaCl , synthetic WIPP brine and synthetic WIPP brine without borate at pC_{H+} 7 (a) and 9 (b).

One inadequately understood component of WIPP brine is borate, even though it comprises a significant portion of the brine, with a concentration near160 mM. To investigate the borate effect on Np speciation in WIPP brine, two additional pC_{H+} 7 and pC_{H+} 9 samples in synthetic WIPP brine without borate were prepared and analyzed by UV-Vis-NIR (Figure 1a and 1b). The Np(V) absorption spectra of synthetic WIPP brine in the absence of borate show the characteristic Np(V) absorption band with a peak maximum of λ_{max} ~982 nm (and a small shoulder at ~990 nm) at pC_{H+} 7 and λ_{max} ~ 983 nm at pC_{H+} 9. This minor peak shift to a higher wavelength could be caused by the presence of weak complexants, including chloride, sulfate, hydroxide, or other brine components, and results in a slightly greater shift than observed for solutions in 5 M NaCl alone.

Maiwald et al. (2020) studied Np(V)-sulfate interactions in aqueous solutions as a function of total ligand concentration (Na_2SO_4), ionic strength ($NaClO_4$), and temperature (T = 20–85 ºC) at pH 4.3 by using UV-Vis-NIR. They reported a single species of $NpO_2(SO_4)^-$ at 983.1 nm through peak deconvolution of the absorption spectra [Maiwald 2020]. The NIR spectra of Np in synthetic WIPP brine (including borate) at pC_{H+} 7 and 9 are also shown in Figure 1a and 1b, where we observe a more pronounced bathochromic shift of the Np(V) absorption band (λ_{max} = 984 nm and 988 nm for pC_{H+} 7 and 9 brines, respectively). The absolute intensity also increases for the pC_{H+} 7 borate-bearing sample, suggesting significant contributions from Np(V)-borate species. However, the intensity of the pC_{H+} 9 sample decreases, signifying the likelihood of Np(V)-borate incorporation into a solid phase.

The Np(V)-borate interaction was probed further using samples containing 10 mM ≤ $[B]_{tot}$ ≤ 100 mM in 5 M NaCl at pC_{H+} 7 and 9 (Figure 2a and 2b). At $[B]_{tot}$ = 10 mM in the 5 M NaCl at pC_{H+} 7 and 9 systems, minimal red shift is observed, indicating the predominance of NpO_2^+. As $[B]_{tot}$ increases, the peak maxima are shifted to higher wavelengths, clearly indicating the formation of a Np(V)-borate complex in 5 M NaCl at pC_{H+}7 and pC_{H+} 9. The shift and broadening of the peak observed at pC_{H+} 9 is more pronounced and suggests the possible formation of more than one Np(V) borate species at higher pC_{H+}.

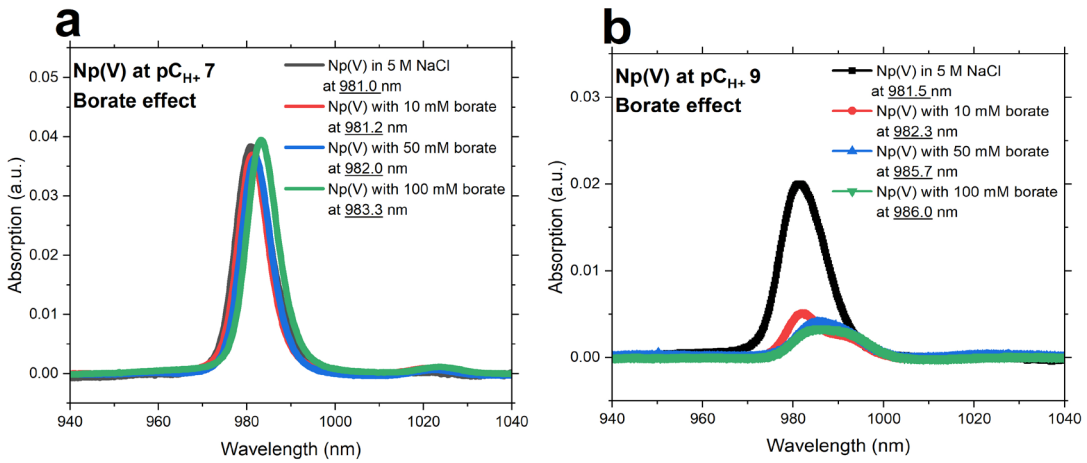


Figure 2. NIR absorption spectra of supernatant solutions in equilibrium with $NpO_2OH_{(am, fresh)}$ as a function of borate concentration in 5.0 M NaCl a) at pC_{H+} 7 and b) at pC_{H+} 9.

The speciation of borate is highly complex. Several borate species, whose concentrations are strongly dependent on pC_{H+}, $[B]_{tot}$, type and concentration of background electrolyte, could behave as possible complexing ligands. Hinz at al. (2020) also studied the interaction of Np with borate in 0.1–5.0 M NaCl and 0.25–4.5 M $MgCl_2$ solutions with 7.2 ≤ pC_{H+} ≤ 10.0 and 0.004 M ≤ $[B]_{tot}$ ≤ 0.16 M using UV-Vis-NIR and other spectroscopic methods. A red shift (≈5 nm) in the Np(V) band at λ = 980 nm indicates the formation of weak Np(V)–borate complexes under mildly alkaline pH_m-conditions. The identification of an isosbestic point supports the formation of at least one Np(V)–borate species in equilibrium with NpO_2^+ in dilute $MgCl_2$ systems. A more complex

aqueous speciation (eventually involving the formation of several Np(V)–borate species) is observed in concentrated $MgCl_2$ solutions [Hinz et al. 2020]. It is especially important to constrain the stoichiometry and stability constants of such Np(V)-borate complexes for the accurate prediction of Np solubility under WIPP-relevant conditions. In the present work, however, the presence of multiple species in WIPP brine and minimal spectral change make it difficult to make any definitive assessments of Np(V) speciation, but the absence of Np(IV) and Np(VI) spectral contributions confirms that no oxidation state changes took place after 60 days.

3.2 Solubility results

3.2.1 Organic effect on solubility of Np(V) in 5 M NaCl and in WIPP brine

Figure 3 shows the solubility of Np in the presence and absence of citrate, acetate, oxalate, and EDTA in undersaturation experiments in synthetic WIPP brines and in 5 M NaCl (a) as a function of time, up to 950 days and (b) as a function of pC_{H+} (7, 9, 11). Strikingly, the solubility of Np is ~2 orders of magnitude higher in 5 M NaCl compared to synthetic WIPP brine. Some variation is seen between samples containing different organics, illustrating the effect of organic complexants on Np solubility, which is more pronounced for the 5 M NaCl system at pC_{H+} 9 after 950 days than in WIPP brine. In particular, the Np-oxalate system demonstrated greater solubility than other organics in 5 M NaCl. When interpreting these results in conjunction with the E_h values, it is observed that in samples containing citrate, the E_h values are significantly lower compared to other organics, indicating more reduced conditions. This suggests that within the sample, Np(V) may be reduced to Np(IV), and this can be explained by the lower solubility of Np(IV) compared to Np(V). Furthermore, the literature contains detailed studies demonstrating that in the presence of citrate, Np(V) is reduced to Np(IV) and U(VI) is reduced to U(IV) [Bonin et al. 2007, Francis and Dodge 2008].

The solubility of Np(V) in WIPP brine shows variability over time. Initially, this difference is observed to be significant, but as time progresses, the effect of organics on Np solubility gradually decreases. Particularly after about one year, the solubility of Np was observed to be in the same order of magnitude. By the end of 950 days, all samples, except for acetate, converge at nearly the same solubility value. Additionally, it was observed that in the initial sampling (two-week sampling), the solubility of Np was lowest in the presence of oxalate, but over time, it followed a different trend compared to other organics. The reason for this is that the amount of oxalate initially used was above the solubility value in WIPP brine at pH 9. In other words, oxalate that precipitated initially in WIPP brine gradually dissolved, suggesting the formation of news complexes with Np.

It was also observed that the solubility of Np increases by up to two orders of magnitude in NaCl systems in the presence of organics, whereas a similar effect is not observed in WIPP brine containing divalent cations such as Mg^{2+} and Ca^{2+} (see Table 1). The most likely explanation for this is that divalent cations in the brine, especially Mg^{2+} and Ca^{2+}, tend to form highly stable complexes with these organic complexing agents, thereby competing with actinides for complex formation and effectively reducing the impact of organic complexation on actinide solubility

[Serne et al. 2002, Hummel et al. 2005, CRA 2019]. Alternatively, cations such as Mg^{2+} and Ca^{2+} can participate in the formation of ternary complexes involving both Np and the organics, and can function as stabilizing counter-ions for negatively charged complexes, thereby promoting the formation of stable ternary or quaternary complexes such as Ca/Mg-RN-L or Ca/Mg-RN-OH-L (RN: radionuclide, L: Ligand) [Felipe-Sotelo et al. 2015, DiBlasi et al. 2021].

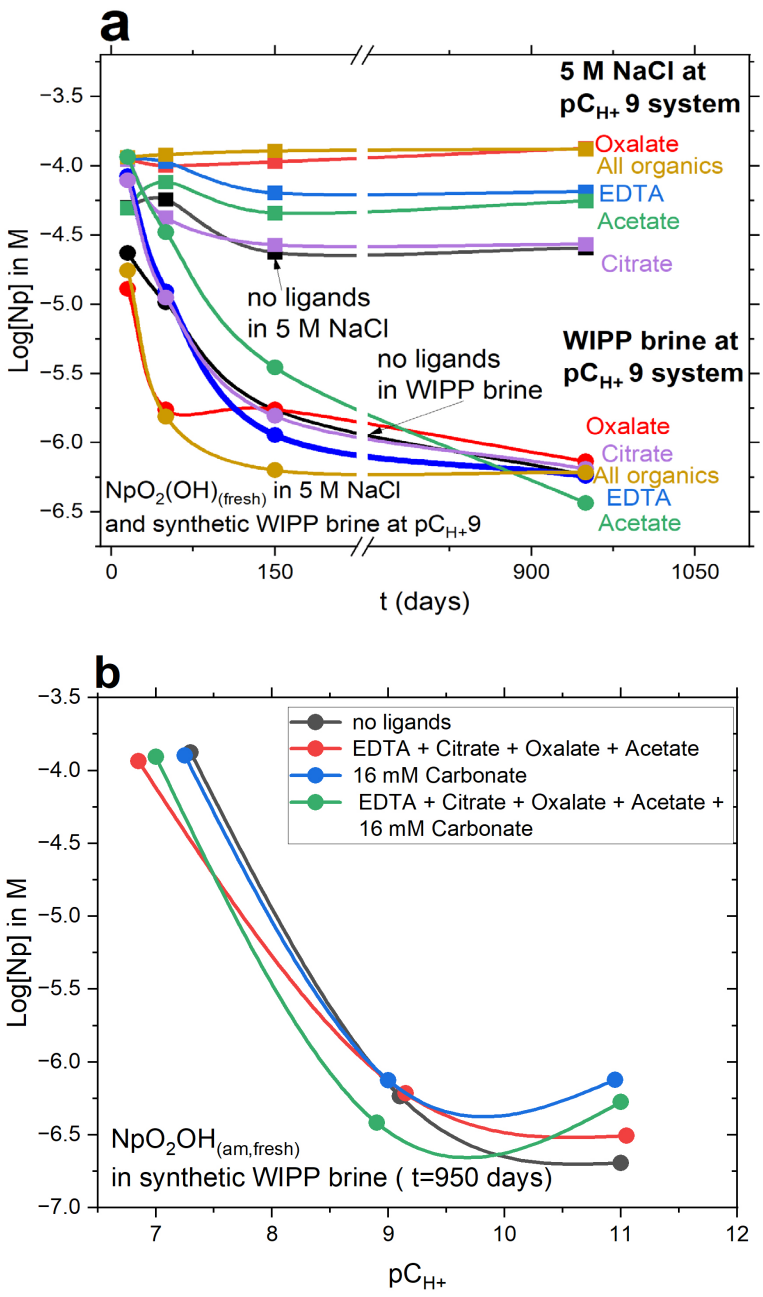


Figure 3. Solubility of $NpO_2(OH)_{(am,\ fresh)}$ in the absence and presence of organic ligands (citrate: 2.30 ×10^{-3} M, acetate: 2.83 ×10^{-2} M, oxalate: 1.13 × 10^{-2} M, EDTA: 7.92 × 10^{-5} M), and carbonate (16 ×10^{-3} M) in synthetic WIPP brine and 5M NaCl solutions as a function of time (a) and pC_{H+} (b). The maximum uncertainty is ± 15 %.

Speciation predictions for Np(V) in 5 M NaCl, including all organic ligands and 16 mM carbonate Domski and Sisk-Scott (2019) calculated the speciation of neptunium (Np) in the presence of organic ligands in GWB using the solubility-controlling solid phase $KNpO_2CO_3(s)$ and the geochemical equilibrium modeling code EQ3/6. The complexation reactions and corresponding stability constants for the expected Np(V) species under WIPP conditions are provided in Table 6. According to their findings, the most significant reaction for Np(V) speciation at $pC_{H+} \cong 9.5$ is the complexation of NpO_2Ac, NpO_2^+, $NpO_2CO_3^-$, and NpO_2Ox^-, with the latter predicted to be the dominant species at $pC_{H+} \cong 9.5$. Our results confirm that organic matter has a time-dependent decreasing effect on Np solubility in WIPP brine. Model calculations suggested that the total concentration of soluble Np species at $pC_{H+} \cong 9.5$ was 4.02×10^{-7} M. A similar Np concentration of 3.84×10^{-7} M was observed in the present experiments (see Table 6) [Domski and Sisk-Scott 2019].

Table 6. Distributions of dissolved Np(V) species in GWB, specifying $KNpO_2CO_3$ as the solubility-controlling solid, as modeled with EQ3/6 geochemical equilibrium modeling code [Domski and Sisk-Scott 2019]

Np(V) species	Concentration (M)	Percent of Solubility
$NpO_2Ac(aq)$	2.35×10^{-7}	58.34%
NpO_2^+	7.05×10^{-8}	17.52%
$NpO_2CO_3^-$	6.48×10^{-8}	16.12%
NpO_2Ox^-	2.68×10^{-8}	6.66%
$NpO_2(OH)(aq)$	3.41×10^{-9}	0.85%
NpO_2Cit^{2-}	1.40×10^{-9}	0.35%
$NpO_2(CO_3)_2^{3-}$	6.26×10^{-10}	0.16%
$NpO_2(OH)_2^-$	6.75×10^{-12}	-
$NpO_2(CO_3)_3^{5-}$	3.61×10^{-12}	-
$NpO_2EDTA_3^-$	8.04×10^{-15}	-
NpO_2HEDTA^{2-}	2.70×10^{-17}	-
$NpO_2H_2EDTA^-$	3.62×10^{-21}	-
Total	**4.02×10^{-7}**	**100.00%**

The effect of pC_{H+} and WIPP-relevant ligands, including carbonate, on Np(V) solubility in synthetic WIPP brine (pC_{H+} = 7, 9, and 11) is summarized in Figure 3b. In simulated WIPP brine, the contribution of organic ligands to Np solubility is minimal across the studied pC_{H+} range, especially at pC_{H+} 7 and 9, with only a slight increase in solubility observed at pC_{H+} 11. This is due to the complexes formed between carbonate and Np at pC_{H+} 11.

Additionally, data obtained from the 5 M NaCl system are presented in Figure 4, using two different thermodynamic databases (ThermoChimie version 11a (TC11a) and THEREDA). The calculations using the modified ThermoChimie and THEREDA databases were both performed in PHREEQC version, using the SIT model for ThermoChimie and the Pitzer model for THEREDA. The results demonstrate that the solubility behavior of Np, both in the presence and absence of organic ligands, is more consistent with predictions based on the aged (crystalline system). This observation is supported by experimental data from amorphous systems, where Np concentrations as high as 10^{-3} M were measured at pC_{H+} 9 [Moog et al. 2015, Blanc et al. 2015, Petrov et al. 2017, Parkhurst and Appelo, 2013].

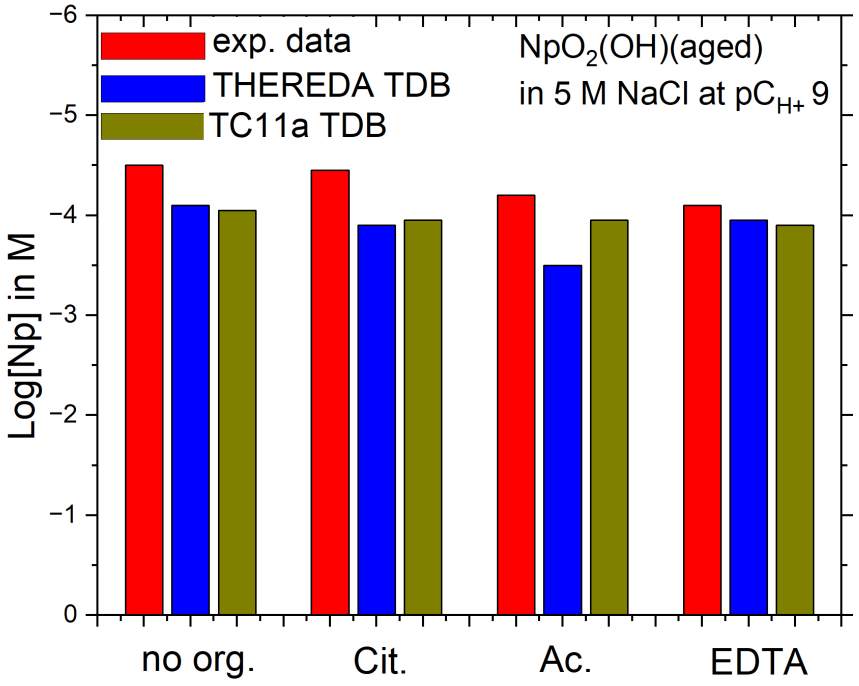


Figure 4. Solubility of $NpO_2(OH)$(aged) in the absence and presence of organic ligands (citrate: 2.30×10^{-3} M, acetate: 2.83×10^{-2} M, EDTA: 7.92×10^{-5} M) in 5 M NaCl solutions at $pC_{H+} \approx 9$ after 950 days. Red bars represent experimental values; blue bars show calculated solubility of $NpO_2(OH)$(aged) using the THEREDA TBD (Thermodynamic database), green bars show calculated solubility using the TC11a (ThermoChimie version 11a) TDB.

3.2.2 Borate effect on Np(V) solubility 5 M NaCl and in WIPP brine

The effect of $[B]_{tot}$ ($0 \leq [B]_{tot} \leq 160$ mM) on Np solubility in 5 M NaCl and synthetic WIPP brines at pC_{H+} 7, 9, and 11 is summarized in Figure 5a and 5b, and includes previous solubility data for $NpO_2(OH)_{(am)}$ [Petrov et al. 2017], $NpO_2(OH)_{(am,\ fresh)}$ and $NaNpO_2$-$borate_{(cr)}$ [Hinz 2020]. The observed neptunium (Np) solubility under alkaline conditions in the absence of borate is in reasonable agreement with the previously reported solubility of NpO_2OH(am) in a 5 M NaCl

solution [Petrov et al. 2017]. The presence of borate had virtually no effect on Np solubility in 5 M NaCl solution or WIPP brine at pC_{H+} 7 and 11. The effect of borate became apparent at pC_{H+} 9, where the concentration of aqueous Np significantly decreased with increasing borate concentration in 5 M NaCl solution. In the presence of $[B]_{tot}$ 160 mM, the solubility limit of Np(V) in 5 M NaCl was more than 3 orders of magnitude lower than that observed in the absence of borate at pC_{H+} 9. The increasing borate concentration, particularly at 160 mM $[B]_{tot}$, reduced Np(V) solubility by more than 3 log units. These results support the formation of Np-borate solid phases controlling solubility at pC_{H+} 9 in 5 M NaCl. Hinz et al. (2020) performed multi-method solid phase characterization using XRD, XPS, SEM–EDS, TEM and XAS to confirm the formation of hitherto unknown Na–Np(V)–borate(cr) solid phases in NaCl [Hinz et al. 2020]. The presence of borate in synthetic WIPP brine at pC_{H+} 9 had a less pronounced effect on Np solubility compared to the NaCl system, with a decrease of less than 0.5 log units observed.

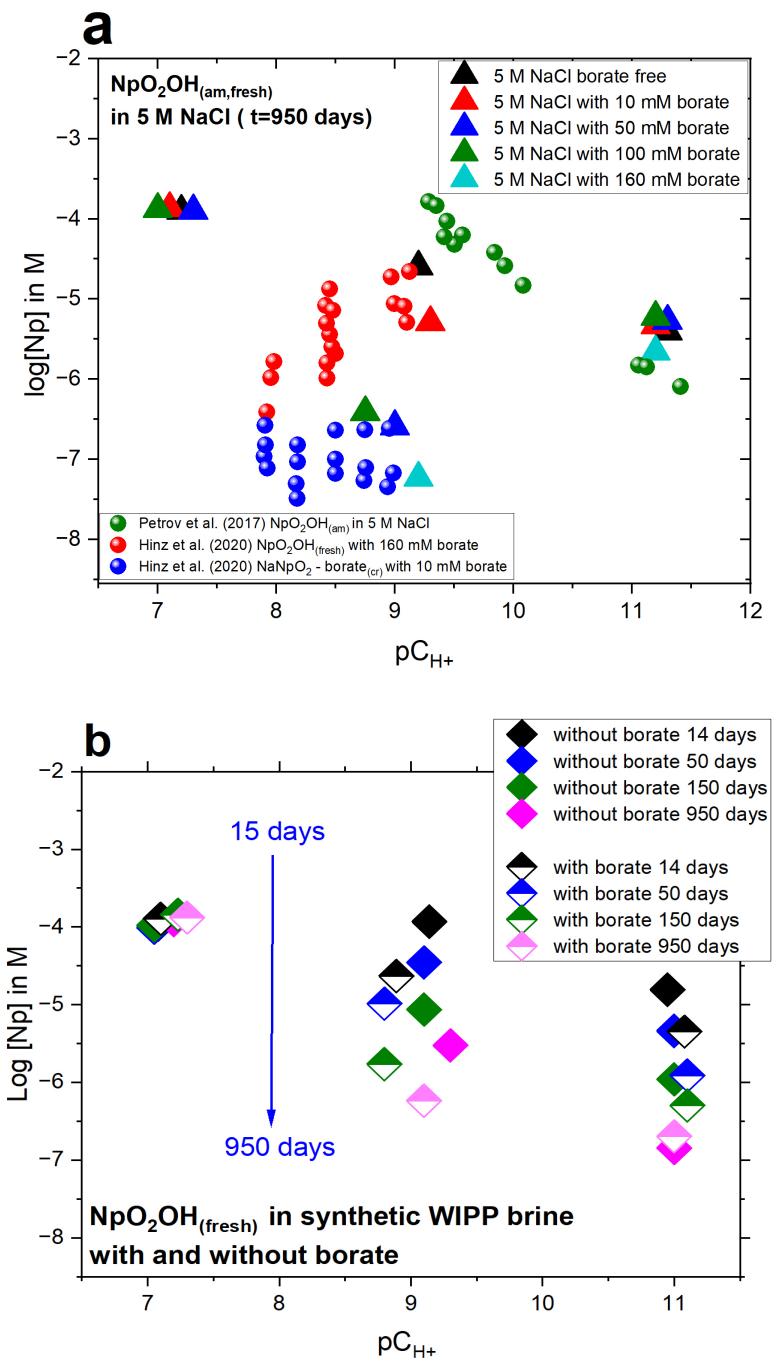


Figure 5. Solubility of $NpO_2(OH)_{(am)}$ in the presence of $[B]_{tot}$ ($0 \leq [B]_{tot} \leq 160$ mM) in 5 M NaCl solutions as a function of pC_{H+} determined in herein (as colored triangles), as well as previous experimental solubility data in the presence and absence of borate [Petrov et al. 2017; Hinz et al. 2020) (half-shaded diamonds) (a). The solubility of $NpO_2(OH)_{(am)}$ in synthetic WIPP brine in the presence and absence of 160 mM M borate as a function of pC_{H+} is also illustrated (b). The maximum uncertainty is ± 15 %.

3.2.3 Carbonate effect on Np(V) solubility in 5 M NaCl

The solubility of $NpO_2(OH)_{(am)}$ was investigated as a function of pC_{H+} and carbonate concentrations of 1 mM ≤ $[CO_3^{2-}]$ ≤ 100 mM in 5 M NaCl and $[CO_3^{2-}]$ = 16 mM in synthetic WIPP brine at pC_{H+} 7, 9, and 11 using an undersaturation experimental approach (Figure 6). Because NaCl solutions do not have a significant pC_{H+} buffering capacity, the addition of sodium carbonate solutions to a 5 M NaCl solution caused a slight changed in the pC_{H+} after initial adjustment. The samples were equilibrated over 950 days.

The solubility of $NpO_2(OH)(am)$ as a function of carbonate concentration (1 mM ≤ $[CO_3^{2-}]$ ≤ 100 mM) in 5 M NaCl and at pC_{H+} 7, 9, and 11 was evaluated using an undersaturation experimental approach, as depicted in Figure 6. In the experiments, no significant variations in $NpO_2(OH)(am)$ solubility were observed at pC_{H+} 7 in 5 M NaCl, whereas a slight decrease in Np concentration was recorded at pC_{H+} 9 with increasing carbonate concentrations. In a comparable investigation by Nitsche et al. (1992), a slight reduction in Np solubility was noted in Yucca Mountain groundwater, where $[CO_3^{2-}]$ = 11.44 mM at pC_{H+} 6.7, in contrast to $[CO_3^{2-}]$ = 2.81 mM at pC_{H+} 7.0. A marked increase in solubility was observed in the sample containing 100 mM carbonate at pC_{H+} 11, attributable to the predominance of carbonate complexation over the hydrolysis of Np under alkaline conditions [Nitsche et al. 1992]. In their study, Runde (2000) explored the solid-liquid equilibria of Np(V) in 5 M NaCl with varying carbonate concentrations and demonstrated that, at low carbonate concentrations, the solubility-controlling solid phase for both curves was the hydrated ternary Np(V) carbonate, $NaNpO_2CO_3•3.5H_2O(s)$. This solid phase initially forms at higher carbonate concentrations and is kinetically favored to precipitate, yet it is thermodynamically unstable. Over time, it undergoes a transformation to the thermodynamically stable equilibrium phase, $Na_3NpO_2(CO_3)_2•nH_2O(s)$. Thus, the observed decrease in Np solubility in the Np-carbonate system implies the conversion to the more stable $Na_3NpO_2(CO_3)_2•nH_2O(s)$ solid phase [Neck et al. 1995, Runde 2000].

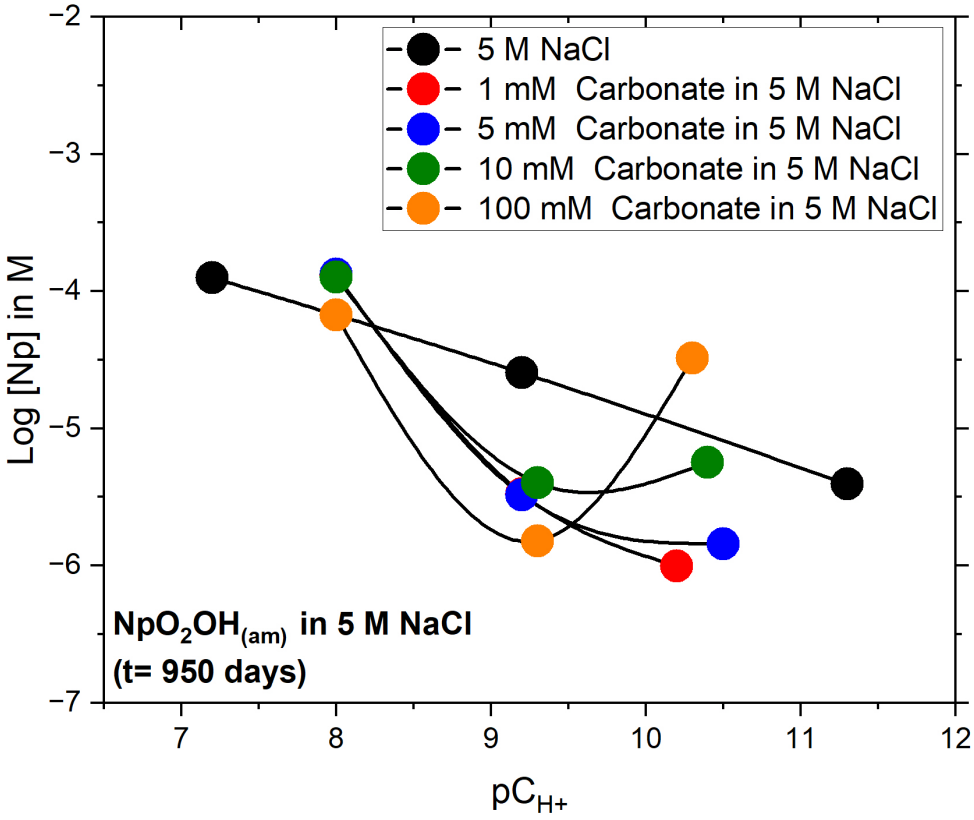


Figure 6. Solubility of $NpO_2(OH)_{(am)}$ in the presence of 1 mM M ≤ $[CO_3^{-2}]_{tot}$ ≤ 100 mM in 5 M NaCl function of pC_{H+}. The results obtained with a maximum error rate of ± 15 %.

3.3 Solid phase speciation by XAS

Np-L_{III} edge XAS spectra were collected from ongoing solubility experiments over a period of approximately 6 months. Figure 7 presents the solid-state reference spectra of Np(IV)O_2(s) and Np(V)O_2(OH)(s), along with the aqueous-phase reference spectra of Np(IV)(aq) and Np(V)(aq). The differentiation between Np(IV) and Np(V) in Np L_{III}-edge XANES spectra is attributed to the presence of axial “yl” oxygen atoms. The manifestation of the Np=O bond in the spectrum appears as a "yl" shoulder in the XANES spectrum (please see Figure 7). As observed in Figures 7 and Table 7, the oxidation state transition of Np from IV to V results in a slight shift of the white line (WL) by approximately 1 eV. Based on the shape and energy position of the WL, the oxidation state determined from Np L_{III}-edge XANES aligns with the solid Np(V) reference samples presented in Figure 8 and Table 7. To quantitatively assess the Np oxidation state, linear combination fitting analysis (LCFA) was performed on the XANES region between 17,585 and 17,700 eV using solid reference spectra of Np(IV) and Np(V). The results indicate that all measured samples consist of 95–99% Np(V), with an associated uncertainty of ±8%. The corresponding LCFA fit, along with the experimental data, is shown in Figure 8.

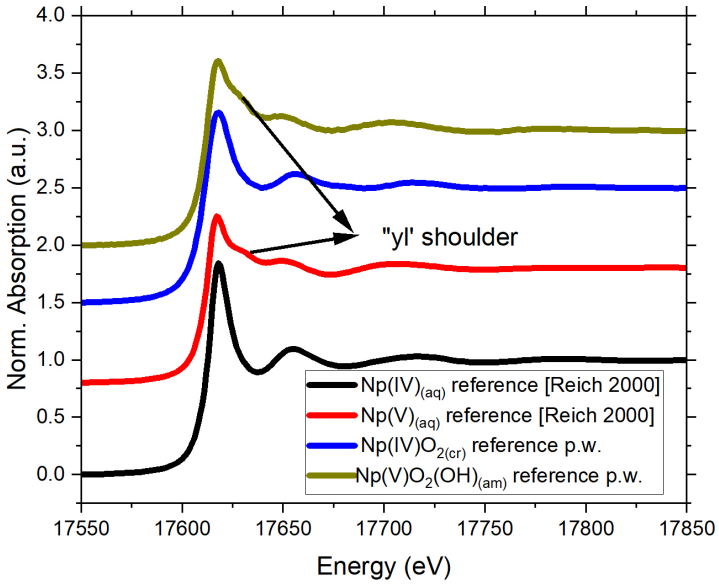


Figure 7. Np L_{III}–edge XANES spectra of Np(IV)O_2(cr) and Np(V)O_2(OH)(am) solid references used in the LCF analysis, as well as aqua reference XANES spectra of Np(IV)O_2^+(aq) and Np(V)O_2^{2+}(aq) are shown for comparison purpose [Reich et al. 2000]. p.w. = present work.

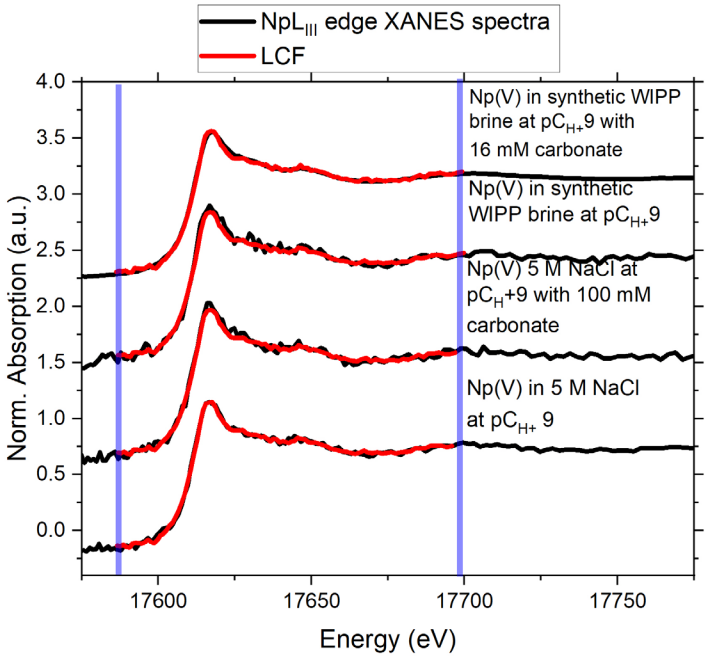


Figure 8. Experimental Np-L_{III}-edge XANES spectra. Each experimental data are compared to corresponding linear combination fits of Np(IV)$O_{2(s)}$ reference and Np(V)O_2(OH)$_{(s)}$ reference. Linear combination fit = red, black = data. The limits of the LCF analysis applied to vertical, purple-colored stripes are shown.

Table 7. Energy positions of the Np L_{III}-edge XANES first inflection point and white line maximum for aqueous and solid Np(V) references and the seven samples investigated in the present work and two reference spectrum (Np(IV) and Np(V)). All values are given in eV (estimated calibration error ΔE ± 0.4 eV). p.w. = present work

Sample matrix	White line maximum (eV)
$Np(IV)_{(aq)}$ refference [Reich et al. 2000]	17 618.0
$Np(V)_{(aq)}$ reference [Reich et al. 2000]	17 617.0
$Np(IV)O_{2(s)}$ reference to LCFA p.w.	17618.2
$Np(V)O_2(OH)_{(s)}$ reference to LCFA and starting material p.w.	17617.2
Np(V) WIPP in 5 M NaCl at pC_{H+} 9	17617.2
Np(V) synthetic WIPP brine at pC_{H+} 9	17616.3
Np(V) 5 M NaCl at pC_{H+} 9 – 100 mM carbonate	17616.5
Np(V) in synthetic WIPP brine at pC_{H+} 9 – 16 mM carbonate	17616.6

In order to investigate the local atomic environment of Np in more detail, Np L_{III}-edge EXAFS spectra for the solid phase equilibrated at $pC_{H^+} \approx 9$ with 16 mM carbonate in synthetic WIPP brine were analyzed. To better distinguish the $Np{=}O_{ax}$ and $Np\text{-}O_{eq}$ interactions that separate Np(V) from Np(IV), the $Np(IV)O_2$(cr) sample was also analyzed and compared with the results. The relevant EXAFS structural parameters are summarized in Table 8. As shown in Figure 9, each sample exhibits different EXAFS patterns. These differences can be attributed to the types of ligands present in the samples and changes in the coordination environments. Curve fitting analysis was challenging due to noise from low Np concentrations and the proximity of equatorial and distant O and C shells to the O=Np=O multiple scattering shell.

For $Np(IV)O_2$(cr), the FT shows a single prominent peak consistent with a single coordination shell consisting of approximately 8 O atoms at a distance of 2.33 Å. Although the hydration number typically assigned to tetravalent actinides is around 8, there have been relatively few direct studies, and the results cover a range of values [Conradson 1998, Choppin 1983]. In addition to this speciation, a Np-Np scattering contribution at longer distances of 3.7 angstroms was observed in EXAFS data, which is attributed to $An(IV)O_2$ precipitation, mostly coordinated by a single shell of 8 O atoms at ~2.36 Å and 12 An(IV) at 3.82 Å [Balboni et al. 2020, Conradson et al. 1998, Allen et al. 1997].

The first shell Np(V) in synthetic WIPP brine at pC_{H+} 9 with 16 mM carbonate in the 1.86–1.89 Å range corresponds to $Np{=}O_{ax}$ atoms, and these values are consistent with the reported 1.82–1.89 Å for the solubility of $Np(V)O_2(OH)$(am) in 5 M NaCl [Petrov et al. 2017] and 1.82–1.86 Å in 4.5 M $CaCl_2$ [Fellhauer et al. 2016].

The second shell in the 2.49–2.59 Å range is likely due to equatorial O atoms, which could be attributed to water molecules or carbonate groups. The narrow range of Np=O bond lengths indicates that the neptunyl units in the samples are well-preserved, and no significant structural

degradation has occurred. The LCFA analysis of XANES spectra and the EXAFS fit for Np-O_{eq} at 2.54 Å confirm the presence of well-ordered neptunyl(V) species.

Additionally, a Np-C interaction was observed at 3.03 Å. To confirm this more clearly, a second modeling was performed without considering the Np-C interaction. Figure 9 shows two different modeling results: one where the Np-C interaction contributes to the model, and one where it does not. As clearly shown in this figure, EXAFS modeling shows that the three-shell model (Np=O_{ax} + Np–O_{eq} + Np–O–C) provides a better fit than the two-shell model (Np=O_{ax} + Np–O_{eq}). This result supports the idea that carbonate groups directly form complexes with Np(V) and play an important role in the coordination environment. In addition, previous solubility studies reported Np–O_{eq} distances of 2.34–2.43 Å [Petrov et al. 2017] and 2.29–2.44 Å [Fellhauer et al. 2016], which are slightly shorter than the observed 2.59 Å values in the presence of carbonate in our investigated sample [Clark et al. 1996]. This suggests that carbonate ions may affect the stability of Np(V) species when they are in the equatorial coordination sphere.

In the presence of carbonate, a contribution from potassium (K) atoms was detected at approximately 4.1 Å in the EXAFS spectrum. Furthermore, in both samples, no formation of polynuclear Np species or Np precipitations, which would lead to a prominent Np–Np peak around 3.7 Å in the FT, was observed.

Previous studies have shown that K-containing Np(V) solid phases may precipitate in alkaline environments. This can occur even though the Na^+ concentration is much higher than the K^+ concentration. The solubility constants determined by Fanghänel et al. (1995) and Novak et al. (1997) show that K-containing Np(V) phases have lower solubility than their Na^+ homologs [Fanghänel et al. 1995, Novak et al. 1997]. In this context, it is believed that a K^+-containing phase has formed in the present study. The presence of K could affect the solubility and environmental mobility of Np(V); therefore, it should be considered an important factor in waste management and long-term radioactive material migration models.

In conclusion, the obtained EXAFS and XANES data highlight the effects of carbonate and K^+ presence on Np(V) structures and provide important information on the long-term geochemical behavior of Np. Future studies should aim to investigate the stability of Np(V) complexes under different ionic strength and pH conditions to better understand their effects on environmental transport pathways.

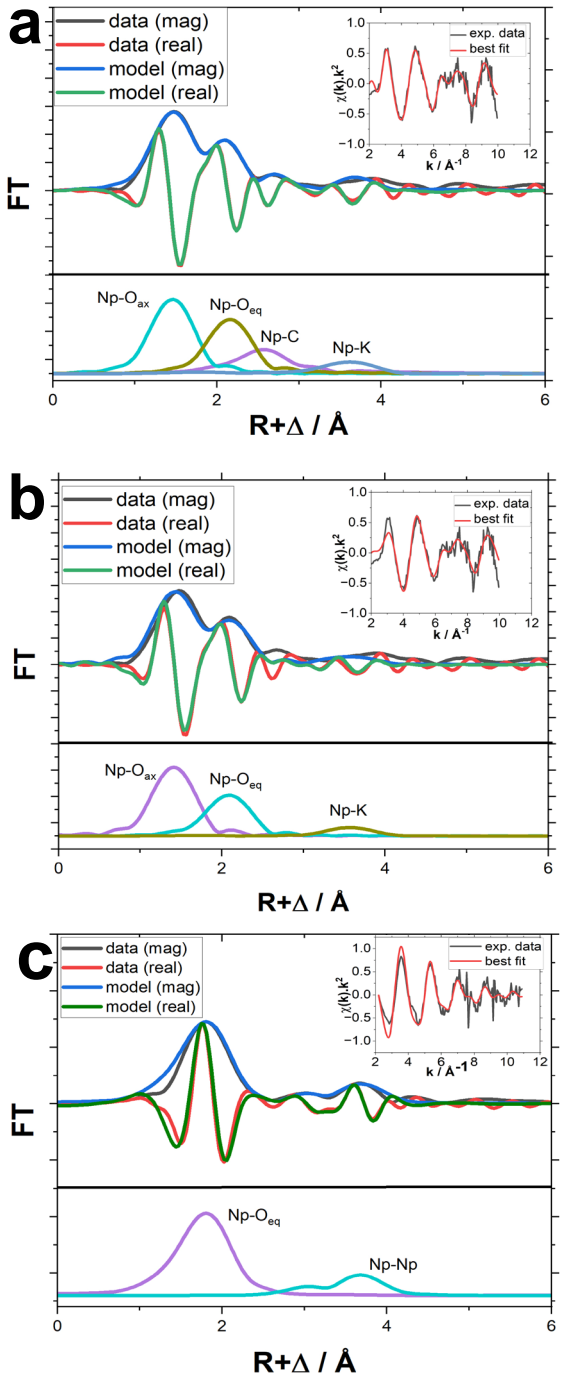


Figure 9. Panel a: Np L_{III}-edge EXAFS spectra with corresponding EXAFS Fourier transform (FT): exp. (experimental) data and best fit of investigated sample Np(V) in synthetic WIPP brine at pC_{H^+} 9 with 16 mM carbonate with considering Np-C shell. Panel b: same sample but not considering Np-C shell during EXAFS calculation. Panel C: Np L_{III}-edge EXAFS spectra with corresponding EXAFS Fourier transform (FT): exp. data and best fit of investigated sample Np(IV)O_2(cr). Data magnitude (mag) (black), model magnitude (blue), data real part (red) and model real part (green). Also shown are single scattering paths.

Table 8. Best-fit of Np L_{III}–edge EXAFS model parameters (S_0^2(k) = 0.9 fixed)

	Np=O_{ax}			Np-O_{eq}			Np-C			Np-K			Np-Np			**ΔE_0**	**Red. error**
	N	R(Å)	σ^2(Å^2)	N	R(Å)	σ^2(Å^2)	N	R(Å)	σ^2(Å^2)	N	R(Å)	σ^2(Å^2)	N	R(Å)	σ^2(Å^2)		
Np(IV)O_2(cr)	-	-	-	8.10*	2.33	0.014	-	-	-	-	-	-	5.55	3.79	0.013	10.6	0.07
NpO_2(OH)(am) + 160 mM [CO_3^{2-}] in WIPP brine at pC_{H+} 9 modeling with carbon	1.27	1.89	0.001	2.58	2.59	0.003	3.59	3.03	0.008	3.03	4.14	0.013	-	-	-	14.7	0.01
NpO_2(OH)(am) + 160 mM [CO_3^{2-}] in WIPP brine at pC_{H+} 9 modeling without carbon	1.17	1.86	0.003	3.46	2.49	0.003*	-	-	-	1.11	4.11	0.004	-	-	-	11.4	0.05
Np(IV)(aq) [Reich et al. 2000]	-	-	-	11	2.39	0.012	-	-	-	-	-	-	-	-	-	-	-
Np(IV)(aq) [Reich et al. 2000]	1.9	1.82	0.023	3.6	2.48	0.061	-	-	-	-	-	-	-	-	-	-	-
[Vitova et al. 2020]	U=O_{ax}			U-$_{Oeq}$			U-C			U-K			U-Np				
	N	R(Å)	σ^2(Å^2)	N	R(Å)	σ^2(Å^2)	N	R(Å)	σ^2(Å^2)	N	R(Å)	σ^2(Å^2)	N	R(Å)	σ^2(Å^2)		
	2.4	1.78	0.001	5.9	2.44	0.004	3.5	2.91	0.004	5	4.02	0.008	-	-	-	3.2	0.7
[Kuzenova et al. 2023]	Np=Oax			N-Oeq			Np-C			N-K			Np-O				
	N	R(Å)	σ^2(Å^2)	N	R(Å)	σ^2(Å^2)	N	R(Å)	σ^2(Å^2)	N	R(Å)	σ^2(Å^2)	N	R(Å)	σ^2(Å^2)		
	2*	1.83	0.003	6*	2.56	0.006	3*	2.96	0.005	6	4.2	0.008	6*	4.28	0.0004	-	0

*Parameter fixed at constant value during fit.

4.0 CONLUSION

This study provides an in-depth, long-term investigation into the solubility behavior and oxidation state of Np in high ionic strength environments relevant to the WIPP. Through a comprehensive series of batch solubility experiments conducted over approximately 950 days under undersaturation conditions, the redox behavior and aqueous speciation of Np in 5 M NaCl and synthetic WIPP brines were systematically characterized as a function of pC_{H^+} (7–11) and in the presence of both inorganic (carbonate, borate) and organic ligands (EDTA, oxalate, citrate, and acetate).

The results consistently demonstrated that Np persists in the +V oxidation state under all tested conditions, as confirmed by both UV-Vis-NIR spectroscopy in solution and XANES analysis of the solid phase. EXAFS spectroscopy further identified the redox-controlling solid phases as $KNpO_2CO_3(s)$ or $K_3NpO_2(CO_3)_2$, which are consistent with solid phases predicted by the WIPP geochemical model. These findings indicate that Np(V) remains the dominant oxidation state in both solution and solid phases under repository-relevant conditions and support the robustness of the current WIPP PA.

The influence of organic ligands varied depending on the chemical environment: in 5 M NaCl, ligand–Np(V) interactions were observed to become more stable over time, whereas in synthetic WIPP brines, kinetic effects initially led to elevated solubility levels, which gradually decreased, indicating the establishment of a dynamic equilibrium. These differences underscore the importance of matrix-specific behavior in actinide–organic interactions, particularly under high ionic strength conditions.

Calculated Np(V) concentrations using the WIPP thermodynamic model (based on the geochemical equilibrium modeling code EQ3/6) were in good agreement with experimental results, indicating that the system approached thermodynamic equilibrium under the experimental conditions.

Overall, this dataset contributes essential empirical validation to the WIPP actinide chemistry model and provides critical insight into the chemical behavior of Np(V) under repository-relevant conditions. These results will inform parameter updates for the CRA-2026 recertification and contribute to refining the conceptual model used in WIPP PA calculations.

5.0 QUALITY ASSURANCE, DATA TRACEABILITY AND DOCUMENTATION

All of the data presented in this report, unless specified otherwise, were generated as Quality Level-1 data, in accordance with the CBFO QAPD. Experiments were performed under the test plan, "Experimental Strategy to Challenge Actinide Solubility Predictions" (LCO-ACP-26, Rev. 1). Descriptions of the experiments can be found in the scientific notebook designated ACP-26-03.

6.0 APPENDIX

6.1 Np(V) UV-Vis-NIR Spectra

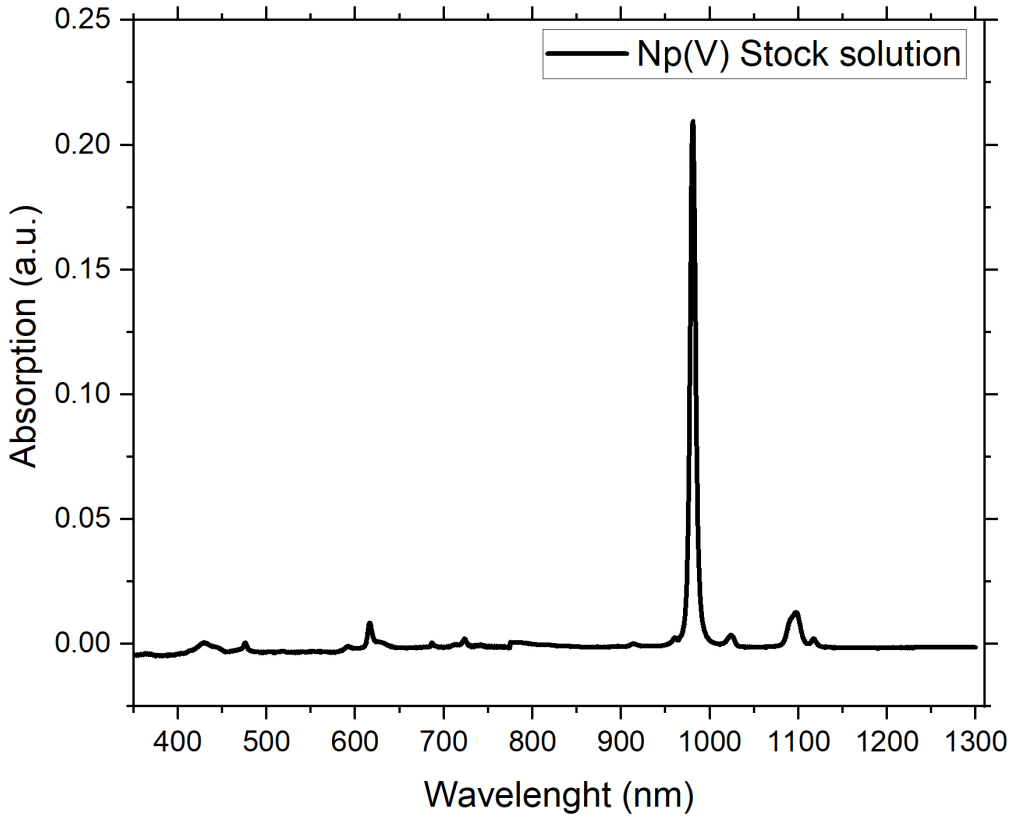


Figure 10: UV-Vis-NIR spectra of Np stock solution in 1 M HCl.

7.0 REFERENCES

Altmaier, M., Metz, V., Neck, V., et al. (2003). Solid-liquid equilibria of $Mg(OH)_2$(cr) and $Mg_2(OH)_3Cl{\cdot}4H_2O$(cr) in the system Mg-Na-H-OH-Cl-H_2O at 25°C. Geochimica et Cosmochimica Acta, 67, 165. https://doi.org/10.1016/S0016-7037(03)00165-0.

Altmaier, M., Gaona, X., Fellhauer, D., et al. (2010). Intercomparison of Redox determination methods on designed and near-natural aqueous systems: FP 7 EURATOM Collaborative Project "Redox Phenomena Controlling Systems" (KIT Scientific Reports; 7572).

Allen, P. G., Bucher, J. J., Shuh, et al. (1997). Investigation of aquo and chloro complexes of UO_2^{2+}, NpO_2^{+}, Np^{4+}, and Pu^{3+} by X-ray absorption fine structure spectroscopy. Inorganic Chemistry, 36(21), 4676–4683. https://doi.org/10.1021/ic970946r.

Al Mahamid, I., Novak, C. F., Becraft, K. A. (1998). Solubility of Np(V) in K-Cl-CO_3 and Na-K-Cl-CO_3 solutions to high concentrations: Measurements and thermodynamic model predictions. Radiochimica Acta, 81, 93–102. https://doi.org/10.1524/ract.1998.81.2.93.

Ankudinov, A. L., Bouldin, C. E., Rehr, J. J., et al. (2002). Parallel calculation of electron multiple scattering using Lanczos algorithms. Physical Review B, 65, 104107. https://doi.org/10.1103/PhysRevB.65.104107.

Balboni, E., Smith, K. F., Moreau, L. M. (2020). Transformation of ferrihydrite to goethite and the fate of plutonium. ACS Earth and Space Chemistry, 4(11), 1993–2006.

Blanc, P., Vieillard, P., Gailhanou, H., Gaboreau, S., Giffaut, E., Marty, N., & Madé, B. (2015). ThermoChimie: A thermodynamic database for waste disposal in clay environments. Applied Geochemistry, 55, 1–15. https://doi.org/10.1016/j.apgeochem.2014.12.014.

Bonin, L., Den Auwer, C., Ansoborlo, E., et al. (2007). Study of Np speciation in citrate medium. Radiochimica Acta, 95(7), 371–379. https://doi.org/10.1524/ract.2007.95.7.371.

Borkowski, M., Lucchini, J. F., Richmann, M. K. (2009). Overview of the actinide chemistry in the WIPP (LA-UR-09-03495). Paper presented at the American Nuclear Society Annual Meeting, Atlanta, GA, United States.

Brush, L.H. (1989). Preliminary Description of the Chemistry of Intergranular Brines from the Salado Formation for the WIPP Supplemental Environmental Impact Statement. Unpublished memorandum. Albuquerque, NM: Sandia National Laboratories.

Choppin, G. R. (1983). Solution chemistry of the actinides. Radiochimica Acta, 32(1–3), 43–54. https://doi.org/10.1524/ract.1983.32.13.43.

Choppin, G. R. (2007). Actinide speciation in the environment. Journal of Radioanalytical and Nuclear Chemistry, 273, 695–703. https://doi.org/10.1007/s10967-007-0933-3.

Clark, D. L., Conradson, S. D., Ekberg, et al. (1996). EXAFS studies of pentavalent neptunium carbonato complexes: Structural elucidation of the principal constituents of neptunium in groundwater environments. Journal of the American Chemical Society, 118(8), 2089–2090. https://doi.org/10.1021/ja953521u.

Conradson, S. D., Al Mahamid, I., Clark, D. L., et al. (1998). Oxidation state determination of plutonium aquo ions using X-ray absorption spectroscopy. Polyhedron, 17(4), 599–602. https://doi.org/10.1016/S0277-5387(97)00467-3.

CRA. (2014). Title 40 CFR Part 191 Subparts B and C Compliance Recertification Application for the Waste Isolation Pilot Plant. U.S. Department of Energy, Carlsbad.

CRA. (2019). Title 40 CFR Part 191 Subparts B and C Compliance Recertification Application 2019 for the Waste Isolation Pilot Plant: Executive Summary. U.S. Department of Energy, Carlsbad.

DiBlasi, N. A., Tasi, A. G., Gaona, X., et al. (2021). Impact of Ca(II) on the aqueous speciation, redox behavior, and environmental mobility of Pu(IV) in the presence of EDTA. Science of the Total Environment, 783, 146988. https://doi.org/10.1016/j.scitotenv.2021.146988.

Domski, P. S. and Sisk-Scott, C. (2019). Prediction of baseline actinide solubilities for CRA-2019 with an updated EQ3/6 Pitzer thermodynamic database, DATA0.FM4. Carlsbad, NM-USA.

Fanghänel, T., Neck, V., Kim, J. I. (1995). Thermodynamics of neptunium(V) in concentrated salt solutions: II. Ion interaction (Pitzer) parameters for Np(V) hydrolysis species and carbonate complexes. Radiochimica Acta, 69(3), 169–178. https://doi.org/10.1524/ract.1995.69.3.169.

Felipe-Sotelo, M., Edgar, M., Beattie, T., et al. (2015). Effect of anthropogenic organic complexants on the solubility of Ni, Th, U(IV), and U(VI). Journal of Hazardous Materials, 300, 553–560. https://doi.org/10.1016/j.jhazmat.2015.07.060.

Fellhauer, D., Altmaier M, Gaona X, et al. (2016) Np(V) solubility, speciation and solid phase formation in alkaline $CaCl_2$ solutions. Part II: Thermodynamics and implications for source term estimations of nuclear waste disposal. Radiochimica Acta 104. https://doi.org/10.1515/ract-2015-2490.

Francis, A. J., & Dodge, C. J. (2008). Bioreduction of uranium(VI) complexed with citric acid by Clostridia affects its structure and solubility. Environmental Science & Technology, 42(23), 8277–8282. https://doi.org/10.1021/es801354k.

Gaona, X., Fellhauer, D., Altmaier, M. (2013). Thermodynamic description of Np(VI) solubility, hydrolysis, and redox behavior in dilute to concentrated alkaline NaCl solutions. Pure and Applied Chemistry, 85, 2049–2065. https://doi.org/10.1351/PAC-CON-12-12-06.

Hinz, K., Altmaier, M., Gaona, X., et al. (2015). Interaction of Nd(III) and Cm(III) with borate in dilute to concentrated alkaline NaCl, $MgCl_2$, and $CaCl_2$ solutions: Solubility and TRLFS studies. New Journal of Chemistry, 39, 4561–4571. https://doi.org/10.1039/c4nj01203h.

Hinz, K., Fellhauer, D., Gaona, X. (2020). Interaction of Np(V) with borate in alkaline, dilute-to-concentrated, NaCl and $MgCl_2$ solutions. Dalton Transactions, 49, 3347–3362. https://doi.org/10.1039/c9dt04430b.

Hummel, W., Anderegg, G., Rao, L., et al. (2005). Chemical thermodynamics of compounds and complexes of U, Np, Pu, Am, Tc, Se, Ni, and Zr with selected organic ligands. Chemical Thermodynamics Series, 9, 1130. OECD Nuclear Energy Agency.

Kaszuba, J. P., Runde, W. H. (1999). The aqueous geochemistry of neptunium: Dynamic control of soluble concentrations with applications to nuclear waste disposal. Environmental Science & Technology, 33, 4427–4433. https://doi.org/10.1021/es990470x.

Kirkes, G. R., Patterson, R. L. (2014). WIPP - February 2014 Operational Events and the Compliance Recertification Application (CRA) 2014.

Kim, J. I. (2006). Significance of actinide chemistry for the long-term safety of waste disposal. Nuclear Engineering and Technology, 38(6), 459–482.

Kropf, A. J., Kemner, K. M., Scheinost, A. C. (2010). The new MRCAT (Sector 10) bending magnet beamline at the Advanced Photon Source. Proceedings of the 10th International Conference, 1234, 299–302.

Kuzenkova, A. S., Plakhova, T. V., Nevolin, I. M., et al. (2023). Formation of Neptunium(V) carbonates: Examining the forceful influence of alkali and alkaline earth cations. Inorganic Chemistry, 62(51), 21025–21035. https://doi.org/10.1021/acs.inorgchem.3c03412.

Lemire, R. J. (2001). Chemical thermodynamics of neptunium and plutonium.

Lierse, C., Treiber, W., Kim, J. I. (1985). Hydrolysis reactions of neptunium (V). Radiochimica Acta, 38(1), 27–28.

Maiwald, M. M., Skerencak-Frech, A., Panak, P. J. (2020). Spectroscopic characterization and thermodynamics of the complexation of Np(V) with sulfate up to 200°C. Spectrochimica Acta Part A: Molecular and Biomolecular Spectroscopy, 240, 118579. https://doi.org/10.1016/j.saa.2020.118579.

Moog, H. C., Bok, F., Marquardt, C. M., & Brendler, V. (2015). Disposal of nuclear waste in host rock formations featuring high-saline solutions – Implementation of a thermodynamic reference database (THEREDA). Applied Geochemistry, 55, 72–84.

Moore, C. R., Free, S. J., & Bynum, R. V. (1999). A thermodynamic model for acetate and lactate complexation with Am(III), Th(IV), Np(V), and U(VI) valid to high ionic strength. In Proceedings of the International Conference on Hazardous Waste: Sources, Effects and Management (Cairo, Egypt, December 12–16, 1998).

Neck, V., Runde, W., Kim, J. I., et al. (1994). Solid-liquid equilibrium reactions of neptunium(V) in carbonate solution at different ionic strengths. Radiochimica Acta, 65, 29–37.

Neck V, Runde W, Kim J. I. (1995) Solid-liquid equilibria of neptunium(V) in carbonate solutions of different ionic strengths: II. Stability of the solid phases. J Alloys Compounds 225. https://doi.org/10.1016/0925-8388(94)07099-7.

Neck, V., Kim, J. I. (2001). Solubility and hydrolysis of tetravalent actinides. Radiochimica Acta, 89, 1–16. https://doi.org/10.1524/ract.2001.89.1.001.

Newville, M. (2013). Larch: An analysis package for XAFS and related spectroscopies. Journal of Physics: Conference Series, 430(1), 012007. https://doi.org/10.1088/1742-6596/430/1/012007.

Nitsche, H., Müller, A., Standifer, E. M., et al. (1992). Dependence of actinide solubility and speciation on carbonate concentration and ionic strength in groundwater. Radiochimica Acta, 58/59, 27–32. https://doi.org/10.1524/ract.1992.5859.1.27.

Novak, C. F., Nitsche, H., Silber, H. B., et al. (1996a). Neptunium(V) and Neptunium(VI) Solubilities in Synthetic Brines of Interest to the Waste Isolation Pilot Plant (WIPP). Radiochimica Acta, vol. 74, no. s1, 1996, pp. 31–36. https://doi.org/10.1524/ract.1996.74.special-issue.31.

Novak, C. F., Borkowski, M., Choppin, G. R. (1996b). Thermodynamic modeling of neptunium(V)-acetate complexation in concentrated NaCl media. Radiochimica Acta, 74(2), 111–116.

Novak, C. F., Al Mahamid, I., Becraft, K. A. (1997). Measurement and thermodynamic modeling of Np(V) solubility in aqueous K_2CO_3 solutions to high concentrations. Journal of Solution Chemistry, 26, 1135–1151. https://doi.org/10.1007/BF02767621.

Parkhurst, D. L., & Appelo, C. A. J. (2013). Description of input and examples for PHREEQC version 3: A computer program for speciation, batch-reaction, one-dimensional transport, and inverse geochemical calculations (Techniques and Methods 6–A43). U.S. Geological Survey. https://doi.org/10.3133/tm6A43.

Petrov, V. G., Fellhauer, D., Gaona, X., et al. (2017). Solubility and hydrolysis of Np(V) in dilute to concentrated alkaline NaCl solutions: Formation of Na-Np(V)-OH solid phases at 22°C. Radiochimica Acta, 105, 2614. https://doi.org/10.1515/ract-2016-2614.

Pokrovsky, O. S., Bronikowski, M. G., Moore, R. C. (1998). Interaction of neptunyl(V) and uranyl(VI) with EDTA in NaCl media: Experimental study and Pitzer modeling. Radiochimica Acta, 80(1), 23–31. https://doi.org/10.1524/ract.1998.80.1.23

Reed, D. T., Wygmans, D. G., Aase, S. B. (1998). Reduction of Np(VI) and Pu(VI) by organic chelating agents. Radiochimica Acta, 82, 109. https://doi.org/10.1524/ract.1998.82.special-issue.109.

Reich, T., Bernhard, G., Geipel, G. (2000). The Rossendorf Beam Line ROBL – A dedicated experimental station for XAFS measurements of actinides and other radionuclides. Radiochimica Acta, 88, 633–637. https://doi.org/10.1524/ract.2000.88.9-11.633.

Runde, W. (2000). Chemical interactions of actinides in the environment. Los Alamos Science, 26.

Runde, W. (2002). Geochemical interactions of actinides in the environment. In P.-C. Zhang & P. V. Brady (Eds.), Uranium, plutonium, transuranics (pp. 33–62). SSSA Special Publication No. 59. https://doi.org/10.2136/sssaspecpub59.c2.

Schramke, J. A., Santillan, E. F. U., Peake, R. T. (2020). Plutonium oxidation states in the Waste Isolation Pilot Plant repository. Applied Geochemistry, 116, 104561. https://doi.org/10.1016/j.apgeochem.2020.104561.

Schott, J., Kretzschmar, J., Acker, M., et al. (2014). Formation of a Eu(III) borate solid species from a weak Eu(III) borate complex in aqueous solution. Dalton Transactions, 43(30), 11516–11528.

Schott, J., Kretzschmar, J., Tsushima, S., et al. (2015). The interaction of Eu(III) with organo-borates: A further approach to understanding the complexation in the An/Ln(III)-borate system. Dalton Transactions, 44(24), 11095–110108.

Serne, R. J., Cantrell, J., Lindenmeier, C. W., et al. (2002). Radionuclide-chelating agent complexes in low-level radioactive decontamination waste; stability, adsorption, and transport potential. NUREG/CR-6758, PNNL-13774. U.S. Nuclear Regulatory Commission, Pacific Northwest National Laboratory.

Silva, R. J., Nitsche, H. (1995). Actinide environmental chemistry. Radiochimica Acta, 70–71, 377. https://doi.org/10.1524/ract.1995.7071.special-issue.377.

Shilov, V. P., Gogolev, A. V., Fedoseev, A. M. (2012). Speciation, stability, and reactions of Np(III-VII) in aqueous solutions. Radiochemistry, 54, 302–310. https://doi.org/10.1134/S1066362212030022.

Snider, A.C. (2003). Verification of the Definition of Generic Weep Brine and the Development of a Recipe for This Brine. ERMS 527505. Carlsbad, NM: Sandia National Laboratories.

Van Soest, G. D. (2018). Performance assessment inventory report 2018. Carlsbad, NM.

Vitova, T., Pidchenko, I., Schild, D. (2020). Competitive reaction of Neptunium(V) and Uranium(VI) in potassium-sodium carbonate-rich aqueous media: Speciation study with a focus on high-resolution X-ray spectroscopy. Inorganic Chemistry, 59(1), 8–22. https://doi.org/10.1021/acs.inorgchem.9b02463.

Wolery, T. J. (2008). Analysis Plan for EQ3/4 Analytical Studies (AP-140, Rev. 0). Sandia National Laboratories, ERMS 548930.

Xiong, Y.-L. (2011). Release of EQ3/6 Database DATAA0FM1. Sandia National Lab. ERMS 555152.

Zachariasen, W. H. (1949). Crystal chemical studies of the 5f-series of elements. Part VI. The Ce_2S_3-Ce_3S_4 type of structure. Acta Crystallographica, 2(3), 1–15.